Cell Reports

Article

BMP7 promotes cardiomyocyte regeneration in zebrafish and adult mice

Graphical abstract

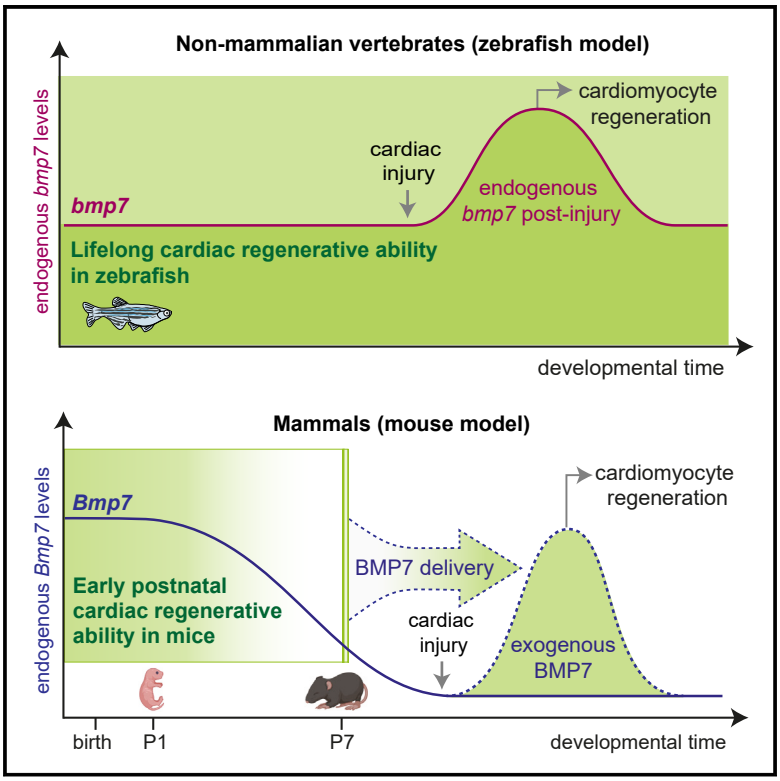

Highlights

- BMP7 expression levels decrease during early postnatal mammalian cardiac development
- Endogenous Bmp7 sustains cardiomyocyte proliferation in zebrafish and in neonatal mice
- BMP7 enhances cardiomyocyte regeneration post-injury in zebrafish and adult mice
- BMP7 induces cardiomyocyte proliferation by activating SMAD5, ERK, and AKT pathways

Authors

Chiara Bongiovanni, Hanna Bueno-Levy, Denise Posadas Pena, ..., Gilbert Weidinger, Eldad Tzahor, Gabriele D'Uva

Correspondence

gabrielematteo.duva2@unibo.it

In brief

Bongiovanni et al. show the role of BMP7 in driving cardiomyocyte proliferation in zebrafish and neonatal mice. As mammalian cardiac development progresses, BMP7, alongside other pro-regeneration factors, declines. However, its augmentation or delivery amplifies cardiomyocyte regeneration following injury in adult zebrafish and mice.

Bongiovanni et al., 2024, Cell Reports *43*, 114162
May 28, 2024
https://doi.org/10.1016/j.celrep.2024.114162

CellPress

Cell Reports

CellPress
OPEN ACCESS

Article

BMP7 promotes cardiomyocyte regeneration in zebrafish and adult mice

Chiara Bongiovanni,[1,2,3] Hanna Bueno-Levy,[4,10] Denise Posadas Pena,[5,10] Irene Del Bono,[1,2,10] Carmen Miano,[1,2,3] Stefano Boriati,[1,2] Silvia Da Pra,[1,2] Francesca Sacchi,[1,2,3] Simone Redaelli,[5] Max Bergen,[6] Donatella Romaniello,[1,2] Francesca Pontis,[7] Riccardo Tassinari,[8] Laura Kellerer,[5] Ilaria Petraroia,[7] Martina Mazzeschi,[9] Mattia Lauriola,[1,2] Carlo Ventura,[1,3] Stephan Heermann,[6] Gilbert Weidinger,[5] Eldad Tzahor,[4] and Gabriele D'Uva[1,9,11,*]

[1]Department of Medical and Surgical Sciences, University of Bologna, via Massarenti 9, 40138 Bologna, Italy
[2]Centre for Applied Biomedical Research (CRBA), University of Bologna, via Massarenti 9, 40138 Bologna, Italy
[3]National Laboratory of Molecular Biology and Stem Cell Engineering, National Institute of Biostructures and Biosystems (INBB), via di Corticella 183, 40128 Bologna, Italy
[4]Department of Molecular Cell Biology, Weizmann Institute of Science, Herzl St. 234, Rehovot 76100, Israel
[5]Institute of Biochemistry and Molecular Biology, Ulm University, Albert-Einstein-Allee 11, 89081 Ulm, Germany
[6]Institute of Anatomy and Cell Biology, Faculty of Medicine, University of Freiburg, Albertstrasse 17, 79104 Freiburg, Germany
[7]Scientific and Technological Pole, IRCCS MultiMedica, via Fantoli 16/15, 20138 Milan, Italy
[8]Eldor Lab, via di Corticella 183, 40128 Bologna, Italy
[9]IRCCS Azienda Ospedaliero-Universitaria di Bologna, via Massarenti 9, 40138 Bologna, Italy
[10]These authors contributed equally
[11]Lead contact
*Correspondence: gabrielematteo.duva2@unibo.it
https://doi.org/10.1016/j.celrep.2024.114162

SUMMARY

Zebrafish have a lifelong cardiac regenerative ability after damage, whereas mammals lose this capacity during early postnatal development. This study investigated whether the declining expression of growth factors during postnatal mammalian development contributes to the decrease of cardiomyocyte regenerative potential. Besides confirming the proliferative ability of neuregulin 1 (NRG1), interleukin (IL)1b, receptor activator of nuclear factor kappa-B ligand (RANKL), insulin growth factor (IGF)2, and IL6, we identified other potential pro-regenerative factors, with BMP7 exhibiting the most pronounced efficacy. Bmp7 knockdown in neonatal mouse cardiomyocytes and loss-of-function in adult zebrafish during cardiac regeneration reduced cardiomyocyte proliferation, indicating that Bmp7 is crucial in the regenerative stages of mouse and zebrafish hearts. Conversely, *bmp7* overexpression in regenerating zebrafish or administration at post-mitotic juvenile and adult mouse stages, *in vitro* and *in vivo* following myocardial infarction, enhanced cardiomyocyte cycling. Mechanistically, BMP7 stimulated proliferation through BMPR1A/ACVR1 and ACVR2A/BMPR2 receptors and downstream SMAD5, ERK, and AKT signaling. Overall, BMP7 administration is a promising strategy for heart regeneration.

INTRODUCTION

In mammals, heart injuries such as those induced by myocardial infarction (MI), result in substantial loss of cardiac muscle cells (cardiomyocytes), which are replaced by fibrotic scar tissue. Due to the very limited regenerative capacity of the adult mammalian heart, this condition often leads to heart failure.[1–6] Currently, effective treatments for cardiac injuries are lacking, highlighting the urgent need to develop therapeutic strategies for cardiac regeneration.

While certain non-mammalian vertebrates, such as zebrafish and some amphibians, exhibit remarkable and lifelong cardiac regenerative capacity,[7–9] significant heart regeneration in several mammalian species has been documented only during embryonic/fetal and neonatal stages.[10–16] Indeed, mammalian cardiac regenerative ability declines rapidly in early postnatal life. In the mouse model, by 1 week after birth, most cardiomyocytes have exited the cell cycle,[17,18] and the heart is unable to regenerate following injuries, resulting in the formation of permanent scars.[11] In adult mammals, cardiomyocyte turnover is extremely low,[19,20] and insufficient to initiate cardiac regeneration.

Reversible dedifferentiation and proliferation of cardiomyocytes play a crucial role in promoting cardiac regeneration in adult zebrafish[21,22] and neonatal mice.[11] Furthermore, endogenous cardiomyocytes represent the primary source of the low rate of cardiomyocyte turnover in adult mammals.[20] Various microenvironmental factors, including neuregulin 1 (NRG1),[23,24] fibroblast growth factor 1 (FGF1),[25] bone morphogenetic protein 10 (BMP10),[26] oncostatin M (OSM),[27,28] tweak,[29] T-reg secreted cytokines,[30] follistatin,[31] vascular endothelial growth factor (VEGF),[32] bone morphogenetic protein 1.3 (BMP1.3),[33] bone morphogenetic protein 2 (BMP2),[34,35] as well as several systemic

factors like thyroid hormones[36] and glucocorticoids,[37] have been shown to modulate dedifferentiation and proliferation of endogenous cardiomyocytes, thereby modulating heart regeneration in adult mammals following severe cardiac injuries.[1–3,38–43] Here, we hypothesize that the decline in expression levels of specific growth factors contributes to the early postnatal loss of cardiomyocyte proliferative and regenerative ability in mammals.

RESULTS

The expression levels of several growth factors rapidly decline in heart tissue during early postnatal mammalian development

In this project we aimed to identify and study the regenerative potential of growth factors exhibiting the most pronounced decline in expression levels in heart tissue during early postnatal development, coinciding with the exit of cardiomyocytes from the cell cycle. To accomplish this, we examined a panel of 117 commercially available growth factors (Table S1) in RNA-sequencing data of hearts isolated from 1-day-old (P1) and 10-day-old (P10) mice.[16] Our analysis revealed that 21 growth factors reduce their expression levels by over 50%, with 12 of them exhibiting a statistically significant decrease (Figure 1A).

We conducted a similar analysis on a second dataset comprising RNA-sequencing data of hearts isolated from 1-day-old (P1) and 9-day-old (P9) mice.[44] This analysis revealed a reduction of at least 50% in expression levels of 15 growth factors (Figure 1B), 13 of which were also identified in the first analysis. By merging the results of the two datasets, we identified a total of 23 factors characterized by a robust decline in expression during early postnatal development. Among these, genes encoding BMP7, interleukin (IL)1RA, NRG1b, CTGF, GDNF, IL23a, BNP (NPPB), insulin growth factor (IGF)2, LGALS7 (GAL7), and LGALS3 (GAL3) were abundantly expressed at P1, while genes encoding for IGFBP1, FGF23, IL1b, IL17b, CXCL17, IL17f, CCL3, CXCL14, GDF5 (BMP14), IL6, soluble receptor activator of nuclear factor kappa-B ligand (sRANKL) (TNFSF1L), and IL10 had low expression levels at P1 (Figures 1A and 1B).

Several growth factors exhibiting a decline in expression during the early mammalian postnatal development promote cell-cycle progression of neonatal cardiomyocytes

Subsequently, we evaluated the mitogenic properties of the 23 selected growth factors. We examined their effects on cell-cycle progression of neonatal cardiomyocytes, which were isolated at postnatal day 1 (P1) and at this stage retain an intrinsic proliferative and regenerative ability reminiscent of the embryonic stage. Considering that the length of the cardiomyocyte S/G2/M phase during development has been estimated to be around 14 h, with a total cell-cycle length of over 24 h,[45] we analyzed the cell-cycle progression of cardiomyocytes over a 48-h time frame using a cumulative BrdU incorporation assay, as previously done.[37] To specifically identify cardiomyocytes, we performed a co-immunostaining for the marker Troponin I. Our data revealed that 18 out of 23 selected growth factors, namely CXCL17, sRANKL, BMP7, GDF5 (BMP14), LGALS7 (GAL7), CCL3, IGF2, IL6, IL1RA, IL17b, CXCL14, IL10, IGFBP, IL1b, NRG1b, LGALS3 (GAL3), IL17f, and GDNF, were able to stimulate the progression of cardiomyocyte cell cycle into the S-phase (Figure 2). Interestingly, NRG1,[23,24,46] IGF2,[47,48] IL6,[49] and sRANKL[47] have previously been reported to promote cardiomyocyte proliferation and heart regeneration, validating our screening approach. IL1b has also been reported to induce cardiomyocyte proliferation,[50] although it may also lead to apoptosis.[51] Importantly, our data unveiled the pro-proliferative potential of other 13 factors. The treatment with CXCL17, BMP7, GDF5 (BMP14), LGALS7 (GAL7), CCL3, and IL1RA produced the most pronounced effects, resulting in more than 1.5-fold increase in cardiomyocyte cell cycle progression compared with untreated controls. IL17b, CXCL14, IL10, IGFBP, LGALS3 (GAL3), IL17f, and GDNF also significantly boosted cardiomyocyte cell cycle progression, albeit to a lesser extent than the previous group of factors (Figure 2).

BMP7 acts as an endogenous growth factor promoting mammalian cardiomyocyte proliferation at the neonatal stage

Based on the screening and analyses described above, we selected six growth factors that exhibited remarkable effects in the BrdU assay: CXCL17, BMP7, LGALS7 (GAL7), GDF5 (BMP14), CCL3, and IL1RA. We did not further analyze IGF2, IL6, and sRANKL, as their ability to promote cardiomyocyte proliferation and cardiac regeneration has already been documented in previous studies.[47,49]

As mentioned earlier, the majority of mammalian cardiomyocytes exit the cell cycle shortly after birth.[17,18] To evaluate the ability of the selected growth factors to promote cell-cycle activity in cardiomyocytes, we analyzed the nuclear immunoreactivity for KI67, a marker for the active phases of the cell-cycle and used cardiac Troponin T as a marker for cardiomyocytes. Our results confirmed that all of the selected growth factors stimulate cardiomyocyte cell-cycle activity, with BMP14 and BMP7, both belonging to the bone morphogenetic protein family, exhibiting the most robust effects (Figure 3A).

During the early postnatal period in mice, most cardiomyocytes undergo DNA synthesis and nuclear division (karyokinesis) without proceeding to cytoplasm division (cytokinesis), resulting in binucleation.[52] Similarly, in humans, most cardiomyocytes undergo DNA synthesis without karyokinesis, resulting in polyploidization.[53] To assess the impact of the selected growth factors on neonatal cardiomyocyte division, we analyzed the staining for Aurora B kinase, which localizes at the equator of the central spindle during late anaphase and at the midbody during cytokinesis.

Our data demonstrated that BMP7 triggers cardiomyocyte cytokinesis (Figure 3B). This effect was further confirmed by time-lapse imaging of neonatal cardiomyocytes labeled with tetramethylrhodamine ethyl ester (TMRE), a fluorescent mitochondrial dye[54] (Figure 3C; Video S1).

By performing negative immunomagnetic selection for cardiac stromal cells, the ability of BMP7 in promoting cardiomyocyte proliferation was also confirmed in cardiomyocyte-enriched cultures (Figures S1A and S1B), suggesting a direct role for BMP7 on neonatal cardiomyocyte proliferation.

CellPress
OPEN ACCESS

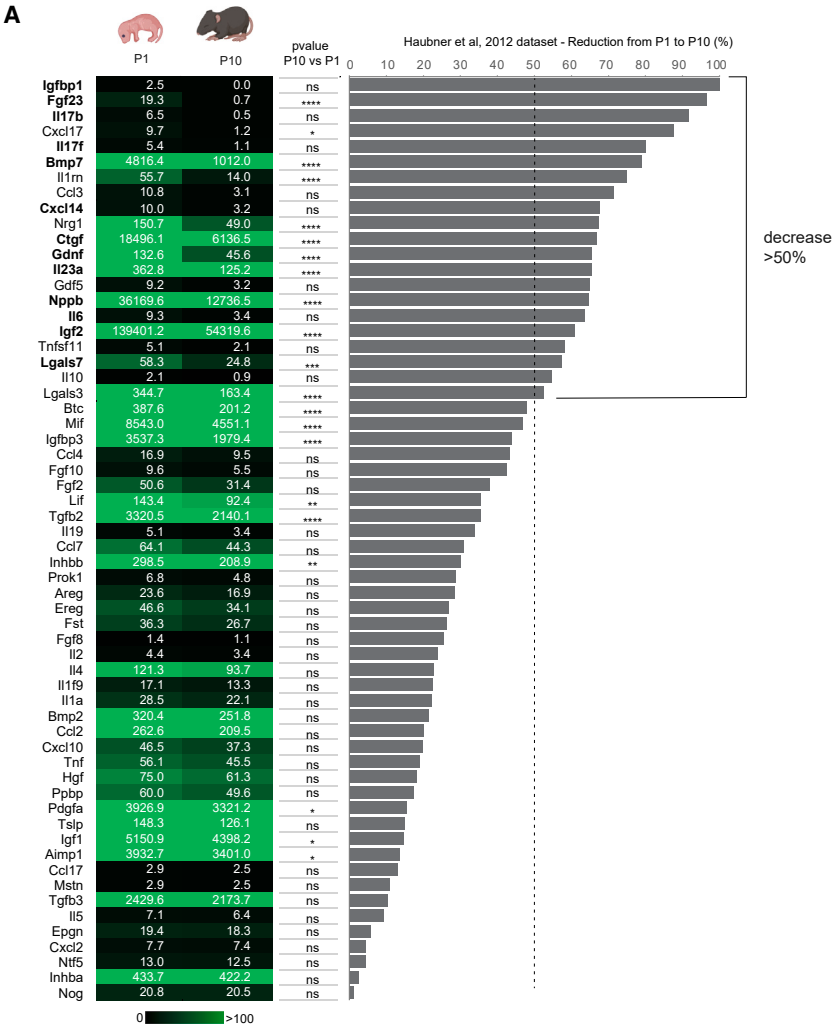

Figure 1. Identification of growth factors with declining expression levels during early cardiac postnatal development

(A and B) mRNA expression levels of growth factors in mouse postnatal day 1 (P1, first column) and postnatal day 9 or 10 (P9 or P10, second column) heart lysates obtained by meta-analysis of RNA-sequencing data,[16,44] along with the calculated decrease from P1 to P10 (or P9) in terms of percentage (graph bar). The values in the first and second columns are presented as mean expression levels of three biological replicates; the *p* value is reported for the reduction from P1 to P10 (or P9) (third column) as follows $^{*}p \leq 0.05$; $^{**}p \leq 0.01$; $^{***}p \leq 0.001$; $^{****}p \leq 0.0001$.

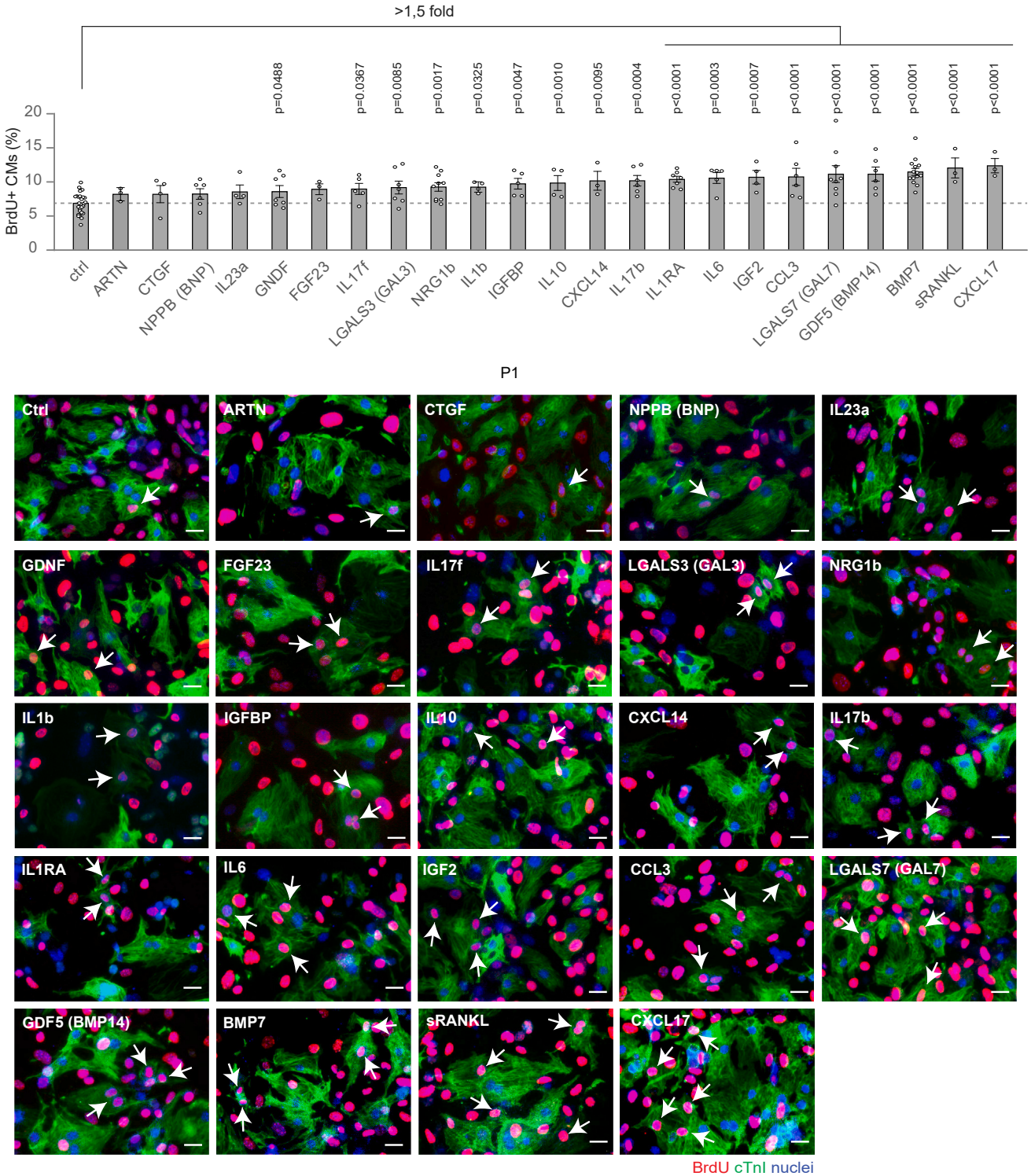

Figure 2. Ability of candidate growth factors to induce neonatal cardiomyocyte cell-cycle progression

Cardiomyocytes isolated from neonatal mice were cultured *in vitro* and stimulated for 48 h with selected growth factors (10 ng/mL), namely ARTN, CTGF, NPPB (BNP), IL23a, GDNF, FGF23, IL17f, LGALS3 (GAL3), NRG1b, IL1b, IGFBP, IL10, CXCL14, IL17b, IL1RA, IL6, IGF2, CCL3, GDF5 (BMP14), LGALS7 (GAL7), BMP7, sRANKL, and CXCL17. Cardiomyocytes were identified by cardiac Troponin I (cTnI) staining and analyzed by immunofluorescence for DNA synthesis (BrdU incorporation assay) (n = 34,914 cardiomyocytes pooled from the analysis of 162 samples); representative pictures are provided; arrows point at proliferating cardiomyocytes; scale bars, 20 μm. The values are presented as mean (error bars show SEM), statistical significance was determined using one-way ANOVA followed by Sidak's test by comparing pairs of treatments (control vs. selected growth factor).

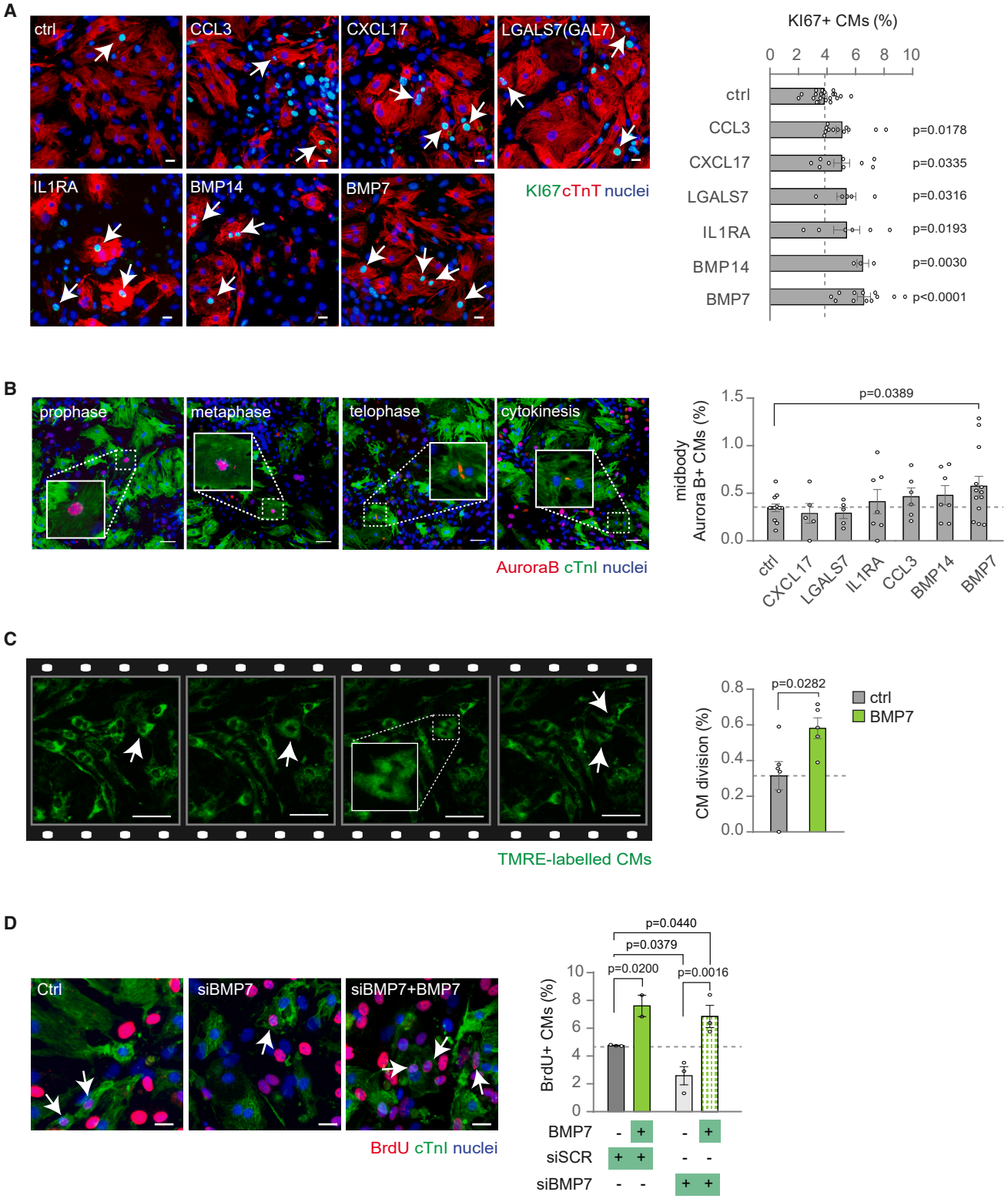

Figure 3. BMP7 robustly induces cell cycle activity and cell division in neonatal mammalian cardiomyocytes

(A and B) Cardiomyocytes isolated from postnatal day 1 (P1) mice were cultured *in vitro* and stimulated for 48 h with selected growth factors (10 ng/mL), namely CCL3, CXCL17, GAL7 (LSGAL7), IL1RA, BMP14, and BMP7. Cardiomyocytes were identified by cardiac Troponin T (cTnT) or Troponin I (cTnI) staining and analyzed by immunofluorescence for (A) cell-cycle activity (KI67) or (B) cytokinesis (midbody Aurora B kinase) (n = 13,961 cardiomyocytes pooled from the

(legend continued on next page)

To evaluate if endogenous BMP7 sustains cardiomyocyte proliferation at the neonatal stage, we knocked down BMP7. The efficiency of BMP7 silencing was confirmed 48 h post-transfection (Figure S1C; Tables S2 and S3). BMP7 knockdown reduced the proliferation of cultured postnatal day 1 (P1) cardiomyocytes, which was restored by exogenous administration of BMP7 (Figure 3D).

Overall, these data indicate that endogenous BMP7 directly promotes cardiomyocyte cell-cycle activity, progression to the S-phase and cell division.

Bmp7 promotes cardiomyocyte proliferation during the spontaneous cardiac regeneration process in zebrafish

The BMP7 protein is encoded by a gene highly conserved across vertebrate species.[55,56] Our previous research in the zebrafish model demonstrated that cardiac injury triggers BMP signaling, and its inhibition prevents cardiomyocyte regeneration.[57] While an increase in the expression of BMP ligands (*bmp2b* and *bmp7a*) has been documented upon injury,[57] the specific role of Bmp7 in cardiomyocyte regeneration in zebrafish has not been previously explored.

To investigate the role of Bmp7 in zebrafish cardiomyocyte regeneration, we analyzed regenerating hearts of zebrafish homozygous for a loss-of-function mutation in the *bmp7a* gene.[58] By injecting wild-type *bmp7a* mRNA into fertilized eggs, we were able to rescue the early embryonic lethality of homozygous mutants,[56] which allowed them to reach adulthood (Figure 4A). We then assessed EdU incorporation at 7 days post cryoinjury (dpi), when cardiomyocyte proliferation is at its peak, and found that cardiomyocyte proliferation within the wound border zone was reduced in *bmp7a*-deficient fish compared with wild-type siblings (Figure 4B).

The zebrafish genome contains two orthologs of human BMP7, *bmp7a* and *bmp7b*, with Bmp7b being more similar to human BMP7 than Bmp7a (~80% compared with ~66% amino acid identity, respectively).[55] Previous studies have shown that the deletion of Bmp ligands including *bmp2b*, *bmp4*, and *bmp7* results in dorsalized phenotypes and early embryonic lethality,[56] while their overexpression induces ventralization.[58] We found that *bmp7a* and *bmp7b* were equally efficient in ventralizing wild-type embryos (Figures S2A and S2B), and that *bmp7b* mRNA could fully rescue *bmp7a* mutant embryos (Figures S2C and S2D). We conclude that zebrafish *bmp7a* and *bmp7b* have similar biological activity in overexpression assays. We thus chose *bmp7b* for further gain-of-function experiments since its sequence is more similar to human BMP7. We generated a transgenic zebrafish line for heat-shock-inducible overexpression of *bmp7b* and concomitant labeling of cardiomyocytes by eGFP (*hsp70L*:bmp7b, *myl7*:eGFP^{af5Tg}).

In uninjured adult hearts of *hsp70L*:bmp7b, *myl7*:eGFP^{af5Tg} fish, the overexpression of *bmp7b* via daily heat shock for 7 days efficiently induced nuclear accumulation of pSmad 1/5/9 in cardiomyocytes (Figures S3A and S3B), but it was not sufficient to induce a significant increase in cycling cardiomyocytes compared with heat-shocked wild-type fish (Figure S3C). In contrast, after cardiac injury, *bmp7b* overexpression significantly increased the number of cycling cardiomyocytes at 7 dpi (Figures 4C and 4D). Together, these results demonstrate that endogenous *bmp7a* sustains cardiomyocyte proliferation during cardiac regeneration in zebrafish, and that further augmentation of *bmp7* levels can enhance this process (Figure S4).

Bmp7 expression levels in cardiomyocytes are reduced during postnatal mammalian development

We examined *Bmp7* expression in cardiac tissues obtained at different stages of postnatal murine development, namely P1, P3, P7, P28, and P56. Our analysis confirmed a significant decrease in *Bmp7* expression during the early postnatal development, and this decline continued beyond that stage (Figure 5A). Using positive and negative immunomagnetic selection for cardiac stromal cells, we also observed that *Bmp7* is more abundantly expressed in cardiomyocytes compared with cardiac stromal cells in neonatal (P1) mice, and that there is a specific reduction in expression within cardiomyocytes during early postnatal development (Figure 5B). To better characterize *Bmp7* expression in the heart tissue, we analyzed publicly available data on sorted cardiac cell populations.[59] These analyses showed that cardiomyocytes and to a lesser extent immune cells express *Bmp7* during the neonatal stage (Figure S5A). Conversely, neonatal fibroblasts and endothelial cells exhibited negligible levels (Figure S5A). Furthermore, *Bmp7* expression levels in cardiomyocytes dramatically declined from the neonatal to the adult stage and was not induced by cardiac injury (Figure S5B). Thus, BMP7 is predominantly produced by neonatal cardiomyocytes, and its expression decreases during early postnatal development. Overall, our data suggest that, in cardiomyocytes, BMP7 is an autocrine factor triggering their proliferation.

Administration of BMP7 stimulates cardiomyocyte proliferation after MI in adult mammals

In mammals, the regenerative ability of cardiomyocytes is dramatically reduced during early postnatal life,[11] coincident with their maturation, binucleation, and cell-cycle exit.[52] To investigate whether BMP7 signaling can induce proliferation in cardiomyocytes after the closure of the regenerative window, we examined the impact of BMP7 treatment at varying concentrations on cardiomyocytes isolated from postnatal day 7 (P7)

analysis of 68 samples in A; *n* = 57,498 cardiomyocytes pooled from the analysis of 55 samples in B); representative pictures are provided; arrows point at proliferating cardiomyocytes; scale bars, 20 μm in (A) and 50 μm in (B).

(C) Quantification and representative images of cell division events (*n* = 11 samples with a total of 5184 cardiomyocytes analyzed) in TMRE-labeled neonatal cardiomyocytes detected in 16-h time-lapse imaging at 15-min intervals *in vitro*; arrows point at cardiomyocytes undergoing cell division; scale bars, 50 μm.

(D) Evaluation of neonatal (postnatal day 1, P1) cardiomyocyte proliferation by immunofluorescence analysis of DNA synthesis (BrdU assay) following knockdown of BMP7 and stimulation with/without BMP7 (10 ng/mL) for 48 h (*n* = 2,480 cardiomyocytes pooled from the analysis of 11 samples). Representative pictures are provided; scale bars, 20 μm; arrows point at cycling cardiomyocytes. The values are presented as mean (error bars show SEM), statistical significance was determined using one-way ANOVA followed by Sidak's test in (A), (B), and (D) (comparison between pairs of treatments; control vs. selected growth factor) and two-sided Student's t test in (C).

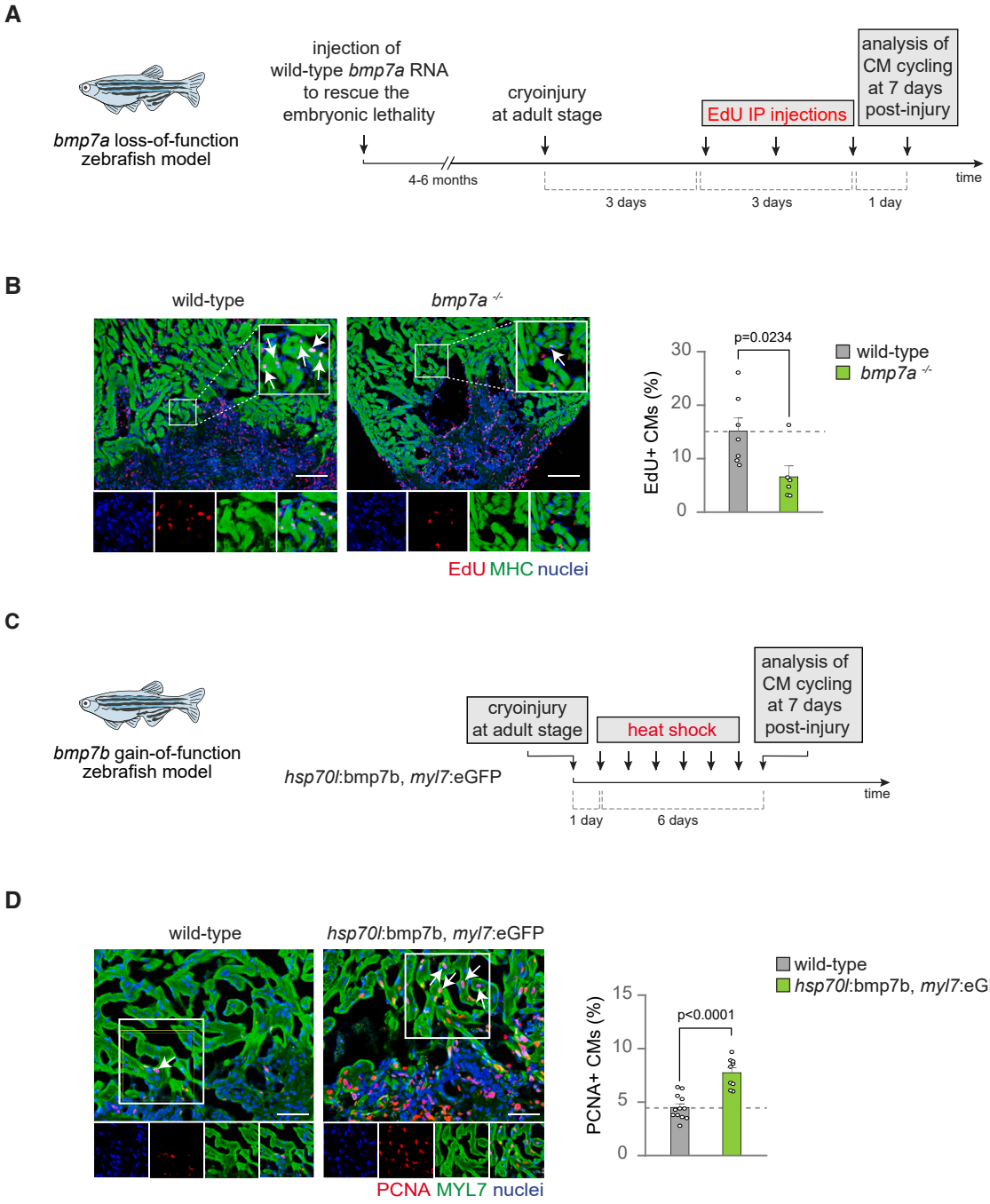

Figure 4. Bmp7 loss- and gain-of-function respectively reduces and increases cardiomyocyte proliferation during zebrafish heart regeneration

(A) Experimental design for the analysis of cardiomyocyte cell cycling in *bmp7a* homozygous mutant fish at 7 days post cryoinjury (dpi).

(B) Immunofluorescence analysis of EdU incorporation and MHC (to identify cardiomyocytes) on cryoinjured hearts of *bmp7a* mutant fish and wild-type siblings. *n* (wild-type) = 7 hearts, three sections per heart, 1158 cardiomyocytes, *n* (*bmp7a*$^{-/-}$) = 6 hearts, three sections per heart, 472 cardiomyocytes. Representative pictures are provided; arrows point at cycling cardiomyocytes; scale bars, 100 μm.

(C) Experimental design depicting the use of a transgenic line allowing for heat-shock-inducible overexpression of *bmp7b* together with constitutive expression of GFP in cardiomyocytes.

(D) Immunofluorescence analysis of PCNA (proliferating cell nuclear antigen) and myosin light chain 7 (MYL7, to identify cardiomyocytes) in heat-shocked *hsp70L*:bmp7b, *myl7*:eGFP^{af5Tg} transgenic and wild-type siblings at 7 dpi. Note that GFP fluorescence is not shown. *n* (wild-type) = 12 hearts, two sections per heart, 421 cardiomyocytes. *n* (*hsp70L*:bmp7b, *myl7*:eGFP) = 9 hearts, two sections per heart, 472 cardiomyocytes. EdU- and PCNA-positive cardiomyocytes in

(legend continued on next page)

mice. Our results show that high doses of BMP7 increase cell-cycle activity (as indicated by KI67 staining) and cell-cycle progression (as indicated by BrdU assay) of P7 cardiomyocytes (Figures 5C and S6A). Additionally, high-dose BMP7 administration robustly increased the number of BrdU+ mononucleated cardiomyocytes (Figure 5D), with a tendency toward a reduction in BrdU+ binucleated cardiomyocytes (Figure S6B). These observations suggest that BMP7 is sufficient to stimulate cell division in juvenile cardiomyocytes, when the regenerative ability is already lost. We then evaluated whether BMP7 is sufficient to induce cardiomyocyte cell-cycle re-entry in adult uninjured mice. For this purpose, we administered BMP7 via intraperitoneal/intravenous injections to adult mouse models for 12 days (Figure S6C). Our data showed a modest increase of adult cardiomyocyte cell-cycle re-entry in BMP7-treated mice (Figure S6D). Interestingly, a recent study has shown that BMP7 administration for 2 weeks after myocardial infarction (MI) has cardioprotective effects, reducing infarct size and improving cardiac function in rats.[60] The suggested mechanism involves the counteraction of transforming growth factor (TGF)-β1 profibrotic signaling pathway.[60] However, the potential of BMP7 to promote the regeneration of adult mammalian cardiomyocytes after a cardiac injury has not been evaluated.

To assess whether BMP7 can stimulate cardiomyocyte proliferation after cardiac injury, we induced MI by permanently ligating the left anterior descending coronary artery in adult mice (3 months old), and we administered BMP7 for 12 days through intravenous/intraperitoneal injections, starting 2 days after MI (Figure 5E). At the end of the treatment (14 days post-MI), we observed an increase in cell-cycle re-entry and proliferation of cycling cardiomyocytes in the infarct border zone (Figures 5F, 5G, and S6E), with a trend toward an increase in remote zones (Figures 5F and 5G). Interestingly, BMP7 delivery modestly decreased cycling of cardiac stromal cells (Figure S7A). The anti-proliferative effect of BMP7 on cardiac stromal cells was also observed in neonatal cardiac cell cultures (Figures S7B and S7C). Overall, our data suggest that BMP7 is a growth factor that specifically triggers mammalian cardiomyocyte proliferation. The decline in its cardiac levels during early postnatal mammalian development contributes to cardiomyocyte cell-cycle exit, whereas its administration after MI in adult mammals triggers cardiac regeneration (Figure S8).

BMP7 stimulates cardiomyocyte proliferation via BMPR1A/ACVR1 type I receptors and BMPR2/ACVR2A type II receptors

BMP7 is a member of the bone morphogenetic proteins (BMPs), which belong to the TGFβ superfamily. The activities of all TGFβ family ligands are mediated by tetramers of serine/threonine kinase receptors, consisting of two type I and two type II receptors.[61–63] BMPs have been reported to signal through ACVRL1, ACVR1, BMPR1A, ACVR1B, and BMPR1B as type I receptors, and BMPR2, ACVR2A, and ACVR2B as type II receptors.[61–63] Specifically, BMP7 has been shown to bind and activate ACVR1, BMPR1A, BMPR2, ACVR2A,[64] BMPR1B,[65] and ACVR2B[66] in different cell types and development stages. To understand the molecular mechanism by which BMP7 regulates cardiomyocyte proliferation, we first analyzed the expression levels of BMP receptors in neonatal murine cardiomyocytes using a publicly available dataset.[59] We found that *Bmpr1a* and *Bmpr2* are the most highly expressed type I and type II BMP receptors, respectively (Figure S9A). *Acvr1b*, *Acvrl1*, *Acvr1*, and *Acvr2a* showed weak expression, whereas *Bmpr1b* and *Acvr2b* were not expressed (Figure S9A) and were excluded from further analyses.

To determine the receptors responsible for the proliferation induced by BMP7, we silenced the genes encoding BMPR1A, ACVR1, ACVRL1, ACVR1B, BMPR2, and ACVR2A in neonatal cultured cardiomyocytes, and then performed a BrdU incorporation assay following BMP7 stimulation. The efficiency of BMP receptor silencing was confirmed 48 h post transfection (Figure S9B; Tables S2 and S3). The results showed that knockdown of BMPR1A, ACVR1, BMPR2 or ACVR2A abolishes the mitogenic effects of BMP7, while knockdown of ACVR1B and ACVRL1 had no significant effect (Figure 6A). These findings suggest that BMP7 promotes cardiomyocyte proliferation through BMPR1A/ACVR1 and BMPR2/ACVR2A receptors, likely forming a tetramer as previously reported in human mesenchymal stem cells.[64]

Canonical SMAD5 transduces the mitogenic signaling of BMP7

BMP ligands activate type II receptors, which phosphorylate the kinase domain of type I receptors and activate multiple downstream pathways.[62,64] The canonical pathway involves receptor-regulated SMAD proteins (R-SMADs), including SMAD1, SMAD5, and SMAD8/9. Once phosphorylated and activated, single or double R-SMADs associate with SMAD4, thus resulting in a heterodimeric or heterotrimeric complex, and translocate into the nucleus.[67]

Therefore, we analyzed the activation of canonical SMAD signaling in cultured neonatal cardiomyocytes stimulated with BMP7 stimulation. Our data showed a transient activation of SMAD1/5/9 in both cardiomyocyte-enriched cultures and cardiac cell cultures, as evidenced by increasing levels of phosphorylated SMAD1/5/9 (*p*-SMAD1/5/9) (Figures 6B, S10A, and S10B). Consistently, nuclear localization of phosphorylated SMAD1/5/9 was higher in cardiomyocytes localized in the infarct border zone of BMP7-treated mice compared with control mice (Figure 6C). The combined knockdown of SMAD1, SMAD5, and SMAD9 completely abolished the mitogenic effect of BMP7, indicating that SMAD1/5/9 signaling is necessary for BMP7-induced cardiomyocyte proliferation (Figure 6D). We also investigated the effects of individual SMAD knockdown on cardiomyocyte proliferation after exposure to BMP7, verifying the efficiency of SMAD silencing 48 h post transfection (Figure S10C). Unexpectedly, our data showed an opposite role for SMAD1 and SMAD5 on cardiomyocyte proliferation. In

(B) and (D), respectively, were counted manually within the border zone of control and transgenic fishes. Each dot represents a different heart (biological replicate), which is the average of the analysis of two to three sections. Representative pictures are provided; arrows point at cycling cardiomyocytes; scale bars, 50 μm. The values in (B) and (D) are presented as mean, error bars show SEM, statistical significance was determined using two-sided Student's t test.

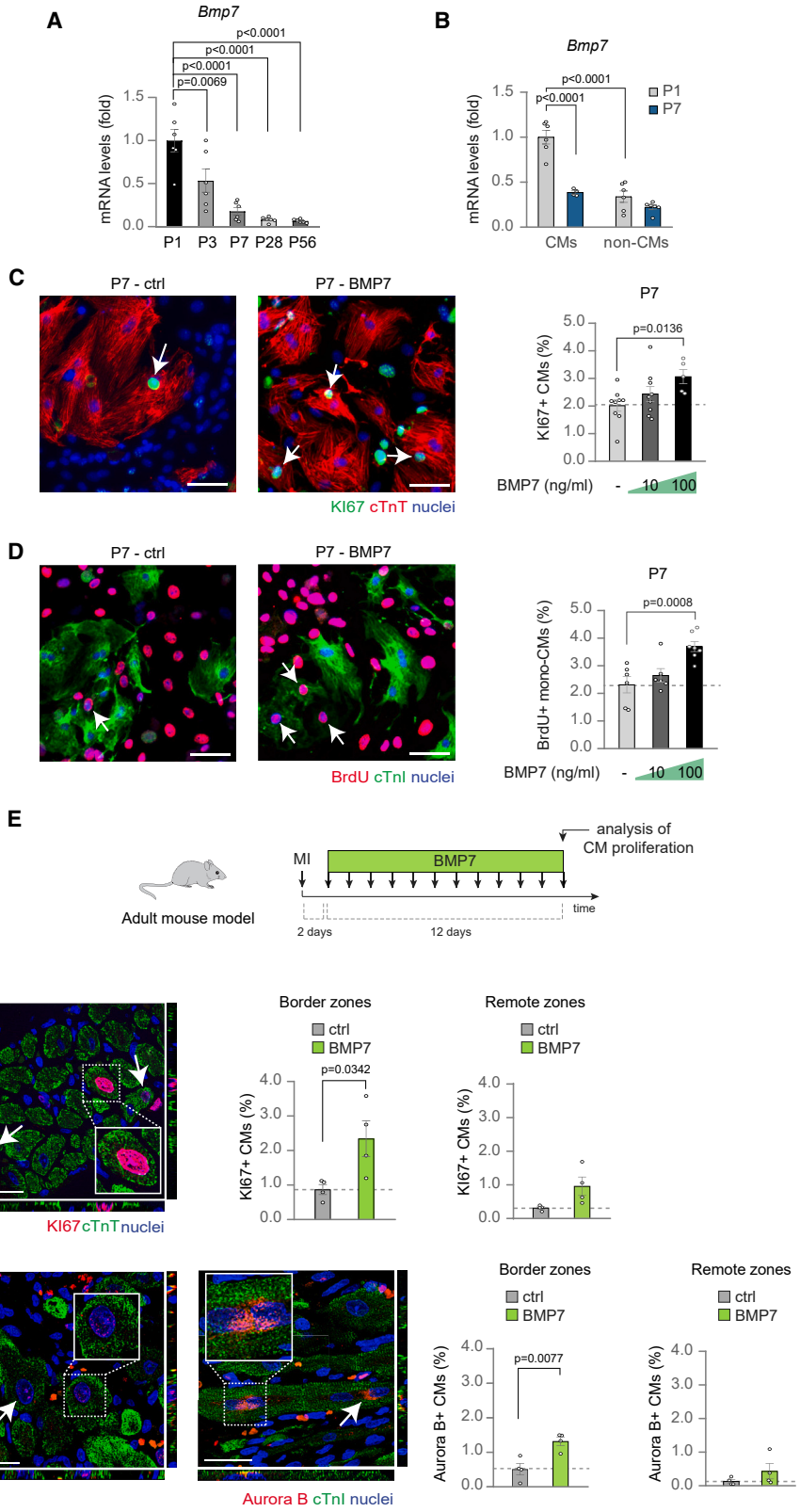

(legend on next page)

absence of BMP7, SMAD1 knockdown significantly increased basal cardiomyocyte proliferation, whereas SMAD5 knockdown trended toward a reduction in cardiomyocyte proliferation. Importantly, SMAD5 knockdown abolished cardiomyocyte proliferation induced by BMP7 exposure, whereas SMAD1 silencing did not affect BMP7 mitogenic activity (Figure 6D). Finally, SMAD9 knockdown did not influence basal or BMP7-induced neonatal cardiomyocyte proliferation (Figure 6C). We further confirmed the activation of SMAD5 in enriched cardiomyocyte cultures, as evidenced by the increase of its phosphorylation levels upon BMP7 stimulation (Figures 6E and S10D).

These data suggest that BMP7 triggers neonatal cardiomyocyte proliferation by activating SMAD signaling. SMAD5 specifically transduces the mitogenic signal of BMP7 in cardiomyocytes, while SMAD1 acts as an endogenous mitogenic suppressor. Additionally, SMAD9 does not appear to play a significant role in mediating BMP7-induced cardiomyocyte proliferation, likely due to its very low expression levels in cardiac muscle cells (Figure S10E).

Non-canonical ERK and AKT pathways mediate BMP7 mitogenic signal transduction

BMP-activated receptors have been shown to activate non-canonical pathways, including those involving ERK and AKT.[68] To investigate the potential role of non-canonical cascades downstream of BMP7 signaling, we evaluated the active phosphorylated isoforms of ERK and AKT. We observed a transient activation of ERK and AKT in cardiac cell cultures after BMP7 stimulation (Figure 7A). By removing stromal cells by immunomagnetic separation, we confirmed that BMP7 treatment increases ERK activation in cardiomyocyte-enriched cultures (Figure S10F). Surprisingly, we could not observe an increase of AKT activation in cardiomyocyte-enriched cultures upon BMP7 treatment, likely because the absence of stromal cells leads to overactivation of AKT at basal levels (Figure S10F), a phenomenon that deserves further investigation. Importantly, our *in vivo* analyses showed increased nuclear immunoreactivity for ERK and AKT in cardiomyocytes within the border zone of BMP7-treated compared with control post-infarcted mice (Figures 7B and 7C).

By using selective ERK and AKT inhibitors, we evaluated whether these pathways play a role in BMP7-induced cardiomyocyte proliferation. Inhibition of AKT and ERK reduced basal cardiomyocyte proliferation (Figure 7D), which is consistent with previous observations.[24] Importantly, BMP7 was unable to enhance cardiomyocyte proliferation when activation of ERK or AKT was blocked (Figure 7D).

Overall, these data suggest that the mitogenic activity of BMP7 in cardiomyocytes is mediated by the canonical SMAD5 and the non-canonical ERK and AKT pathways (Figure 7E).

DISCUSSION

Several mitogens sustain the proliferation of cardiomyocytes during prenatal development and their administration has been explored as a strategy to restore the mitogenic potential of these cells, which is almost completely lost during the early postnatal life in mammals.[1–3,39–43] In this study, we hypothesized that the declining expression of growth factors prompts cardiomyocytes to exit the cell cycle, diminishing the cardiac regenerative ability.

Consistent with our hypothesis, our data show that 18 of 23 identified growth factors with diminishing expression levels during early postnatal mouse cardiac development effectively promote the proliferation of neonatal cardiomyocytes. Notably, some of these growth factors, such as NRG1b,[23,24,46] IL6,[49] IGF2,[47,48] and sRANKL[47] and IL1b,[50] have been previously reported to possess pro-regenerative properties.

Our study also led to the identification of other growth factors exerting a pro-proliferative effect on cardiac muscle cells, including CXCL17, BMP7, GDF5 (BMP14), LGALS7 (GAL7), CCL3, IL1RA, IL17b, CXCL14, IL10, IGFBP, LGALS3 (GAL3), IL17f, and GDNF. Although NPPB, CTGF, IL23a, FGF23, and ARTN did not significantly promote cardiomyocyte proliferation, it is possible that higher dosages, longer treatments, or combined administrations with these factors may still have a proliferative effect. Moreover, BMP7 exhibited the most potent induction of cardiomyocyte cell division. Notably, our study suggests that endogenous production of BMP7 sustains

Figure 5. BMP7 administration stimulates the proliferation of mammalian cardiomyocytes at juvenile stage and in adult life following myocardial infarction

(A) *Bmp7* mRNA expression levels in heart lysates from postnatal day 1 (P1), 3 (P3), 7 (P7), 28 (P28), and 56 (P56) mice (n = 6 hearts per developmental stage) as determined by qRT-PCR and shown relative to the level at P1.

(B) *Bmp7* mRNA expression levels in cardiomyocytes and stromal cells isolated from postnatal day 1 (P1) and postnatal day 7 (P7) hearts and separated by immunomagnetic separation (n = 10 samples for cardiomyocytes and 12 for stromal cells).

(C and D) Immunofluorescence analysis of (C) KI67 and cardiac Troponin T (cTnT) or (D) BrdU incorporation and cardiac Troponin I (cTnI) in postnatal day 7 (P7) total or mononucleated cardiomyocytes following stimulation with BMP7 at 10 and 100 ng/mL for 48 h (for KI67/cTnT staining a total of 5,553 cardiomyocytes pooled from 23 samples have been analyzed; for BrdU/cTnI staining a total of 2843 cardiomyocytes pooled from 19 samples have been analyzed); representative pictures are provided; arrows point at cycling cardiomyocytes; scale bars, 50 μm.

(E) Experimental design for the analysis of cardiac regeneration following ligation of the left anterior descending coronary artery in adult mice (3 months old).

(F and G) *In vivo* evaluation of adult cardiomyocyte proliferation by immunofluorescence analysis of (F) KI67 and cardiac Troponin T (cTnT) or (G) Aurora B kinase and cardiac Troponin I (cTnI) in the border and remote zones of heart sections 14 days post myocardial infarction, following daily injection of BMP7 or water as control (n = 8 mice; for KI67/cTnT staining a total of 14,345 cardiomyocytes have been analyzed in the border zones and 23,085 cardiomyocytes in the remote zones; for Aurora B/cTnI staining a total of 10,088 cardiomyocytes have been analyzed in the border zones and 14,242 cardiomyocytes in the remote zones). Each dot represents a different heart (biological replicate), which is the average of the analysis of two to three sections. Representative pictures show images taken by confocal microscopy showing the xy maximum intensity projection of the stacks acquired from the sample (the slices view on the bottom and left of each panel represent the xz and yz stacks, respectively); arrows point at proliferating cardiomyocytes; scale bars, 25 μm. The values in (A), (B), (C), (D), (F), and (G) are presented as mean (error bars show SEM); statistical significance was determined using one-way ANOVA followed by Sidak's test in (A), (B), (C), and (D) (comparison between pairs of treatments; control vs. BMP7) or using two-sided Student's t test in (F) and (G).

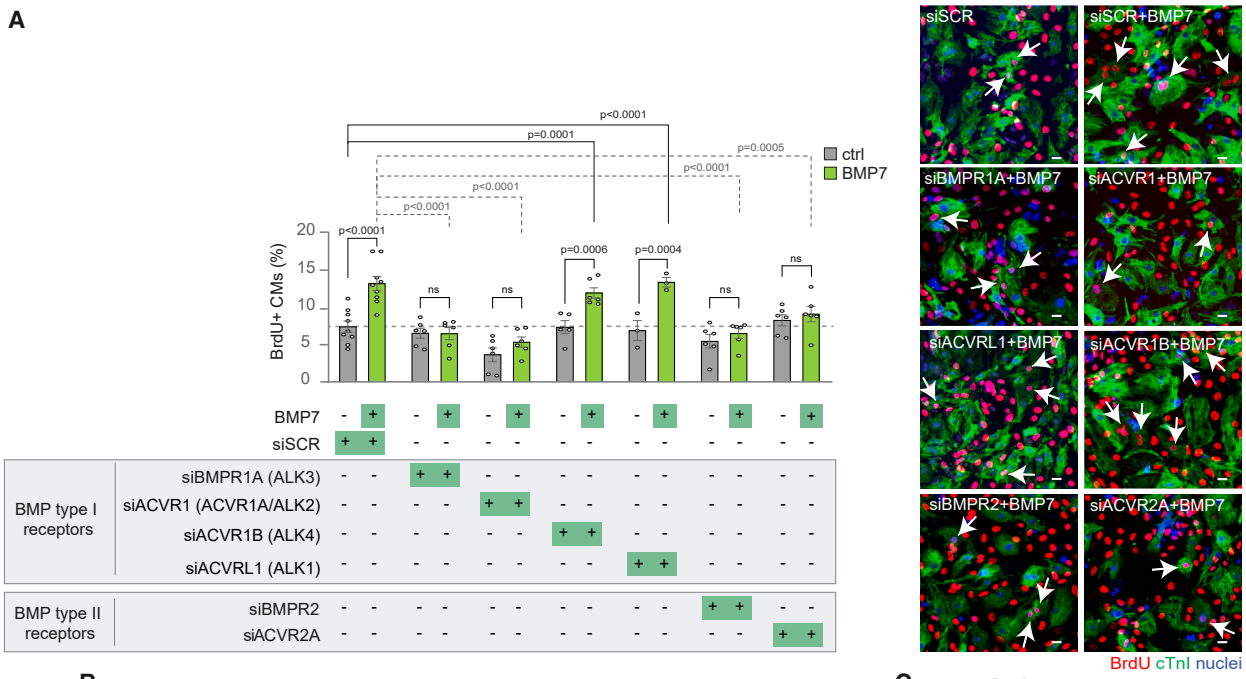

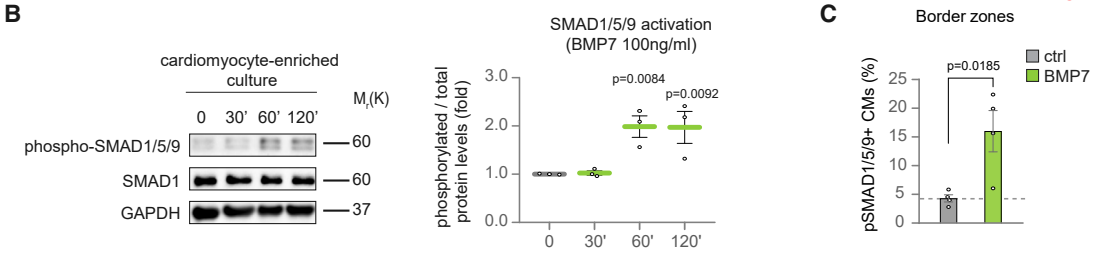

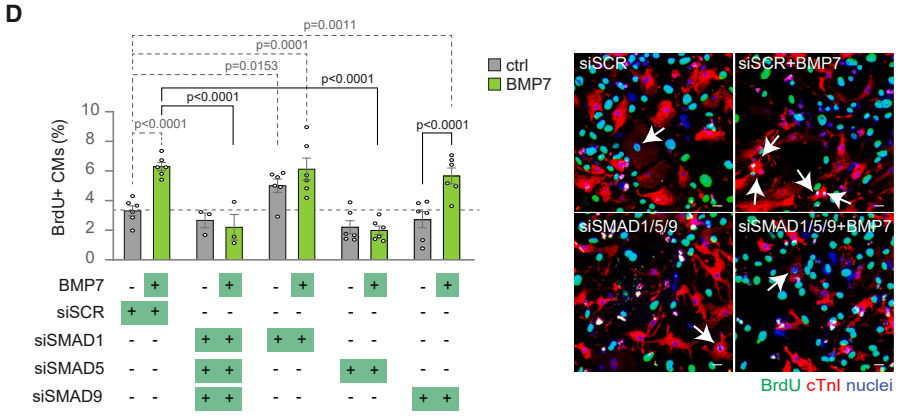

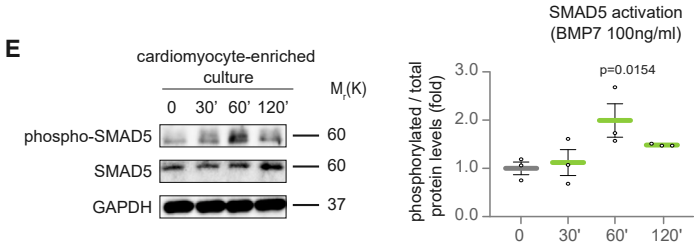

(legend on next page)

cardiomyocyte proliferation at the neonatal stage, as evidenced by BMP7 knockdown experiments. Our data also suggest that neonatal cardiomyocytes express *Bmp7* more abundantly than other cardiac cell populations. Thus, BMP7 appears to be an autocrine proliferative factor for cardiomyocytes, whose expression levels dramatically decline during the early postnatal life in mammals.

BMP7 has been shown to play an anti-fibrotic and anti-inflammatory role in various tissues, including the heart.[60,69–78] BMP7 treatment has been shown to reduce cardiac fibrosis in models of pressure overload,[71,72] diabetic cardiomyopathy,[69,70] and other cardiac genetic pathologies[75] and heart failure models.[76] Dampening of TGF-β pro-fibrotic signaling has been identified as the mechanism by which BMP7 counteracts myocardial fibrosis.[79] Administration of BMP7 after MI in rat models has been shown to reduce scar size and improve cardiac function.[60] Our results suggest that BMP7, in addition to its anti-inflammatory and anti-fibrotic activities, also directly promotes cardiomyocyte regeneration.

Interestingly, BMP7 did not show significant changes in expression levels after MI in neonatal or adult mice. In line with the rationale of our initial screening, these findings suggest that the proliferative and regenerative ability of the neonatal mammalian heart depends at least in part on factors driving the physiological prenatal proliferation of cardiomyocytes, which are highly expressed at the neonatal stage and are not further upregulated in response to cardiac injury. Interestingly, adult zebrafish can re-activate some of these factors, such as *bmp7a*,[57] while adult mice do not (as observed in this study). These observations may partially explain why fish regenerate at adulthood while mice cannot. Nevertheless, screening of growth factors upregulated in regenerating hearts could serve as an alternative strategy for the identification of additional cardiac regenerative factors.

The BMP7 gene is highly conserved among vertebrate species. The importance of BMP signaling in cardiac regeneration was previously documented in the zebrafish model. Activation of the Bmp/Smad pathway occurs after cardiac injury and Bmp inhibition prevents zebrafish cardiomyocyte regeneration.[57] Our study identifies Bmp7a as an endogenous factor that supports cardiomyocyte proliferation during zebrafish cardiac regeneration and demonstrates that increasing *bmp7* expression is sufficient to enhance cardiomyocyte cell cycling during heart regeneration. Another member of the BMP family, BMP14 (GDF5), also exhibited a decline in expression in mice during the early postnatal period in one of the two datasets analyzed (see Figure 1A) and its administration promoted cardiomyocyte cell-cycle activity (see Figures 2, 3A, and 3B). Increased expression of BMP14 after MI has been reported to stimulate cardiomyocyte survival in the mouse model,[80] but its potential role in cardiomyocyte regeneration has not been evaluated.

Notably, *bmp2b* is also upregulated after cardiac injury in the zebrafish model and its overexpression has been demonstrated to enhance zebrafish cardiomyocyte proliferation.[57] Interestingly, in the mouse model, we observed a trend toward a reduction of *Bmp2* during the early postnatal period (see Figure 1A). BMP2 administration has been shown to induce neonatal cardiomyocyte proliferation *in vitro* and to reduce cardiomyocyte apoptosis after MI in adult mice.[34,35,81] However, its potential to trigger mammalian cardiac regeneration remains unexplored.

Our study also elucidated the molecular mechanism underlying the mitogenic action of BMP7, identifying the receptors and downstream canonical and non-canonical signaling pathways. We found that two type I receptors (BMPR1A-ACVR1) and two type II receptors (BMPR2-ACVR2A) are crucial for mediating the mitogenic effect of BMP7 on cardiomyocytes, suggesting that a tetramer transduces BMP7 mitogenic signaling. Downstream mediators are canonical SMAD5, but not SMAD1 that exerted a paradoxical opposite effect, as well as non-canonical ERK and AKT pathways. While ERK appears to be directly activated in cardiomyocytes following BMP7 treatment, AKT activation seems indirect and dependent on the presence of stromal cells, a phenomenon that requires further investigations.

Furthermore, our study revealed that BMP7 reduces the proliferation of cardiac stromal cells both *in vitro* and *in vivo* after MI. This finding aligns with the previously reported anti-proliferative effect of BMP7 on lung fibroblasts.[82] Given that fibroblasts

Figure 6. BMP7 induces cardiomyocyte proliferation through BMPR1A/ACVR1 and ACVR2/BMPR2 receptors and canonical SMAD5 signaling

(A) Evaluation of the role of BMP receptors in BMP7-induced cardiomyocyte proliferation by immunofluorescence analysis of DNA synthesis (BrdU assay) in neonatal (postnatal day 1, P1) cardiomyocytes following BMPR1A, ACVR1, ACVR1B, ACVRL1, BMPR2, and ACVR2A knockdown, upon BMP7 stimulation at 10 ng/mL for 48 h (n = 23,895 cardiomyocytes pooled from the analysis of 83 samples); representative pictures are provided; scale bars, 20 μm, arrows point at proliferating cardiomyocytes.

(B) Western blot analysis of phospho-SMAD1/5/9, SMAD1, and GAPDH protein levels in enriched neonatal cardiomyocytes, separated from stromal cells by immunomagnetic separation, following BMP7 stimulation at 100 ng/mL for 30, 60, and 120 min (n = 3 replicates per condition). GAPDH protein levels are provided as second loading control (see also Figures S10A).

(C) Immunofluorescence analysis for phospho-SMAD1/5/9 and cardiac Troponin T (cTnT) in the border zones of heart sections 14 days post myocardial infarction, following daily injection of BMP7 or water as control (n = 8 mice; a total of 8,342 cardiomyocytes have been analyzed). Phospho-SMAD1/5/9 positive cardiomyocytes in tissue sections were counted within border zones; every dot represents a different heart (biological replicate), which in turn has been calculated as average of the analysis of one to two sections.

(D) Immunofluorescence analysis of DNA synthesis (BrdU assay) and cardiac Troponin I (cTnI) on neonatal (postnatal day 1, P1) cardiomyocytes following SMAD1, SMAD5, and SMAD9 knockdown, alone or in combination, upon BMP7 stimulation at 10 ng/mL for about 48 h (n = 19,167 cardiomyocytes pooled from the analysis of 54 samples); representative pictures are provided; scale bars, 20 μm, arrows point at proliferating cardiomyocytes.

(E) Western blot analysis of phospho-SMAD5, SMAD5, and GAPDH protein levels in enriched neonatal (postnatal day 1, P1) cardiomyocytes, separated from stromal cells by immunomagnetic separation, following BMP7 stimulation at 100 ng/mL for 30, 60, and 120 min (n = 3 replicates per condition). GAPDH protein levels are provided as second loading control (see also Figures S10D). The values in (A)–(E) are presented as mean (error bars show SEM); statistical significance was determined using one-way ANOVA followed by Sidak's test (comparison between pairs of treatments) in (A), (B), (D), and (E); and using two-sided Student's t test in (C).

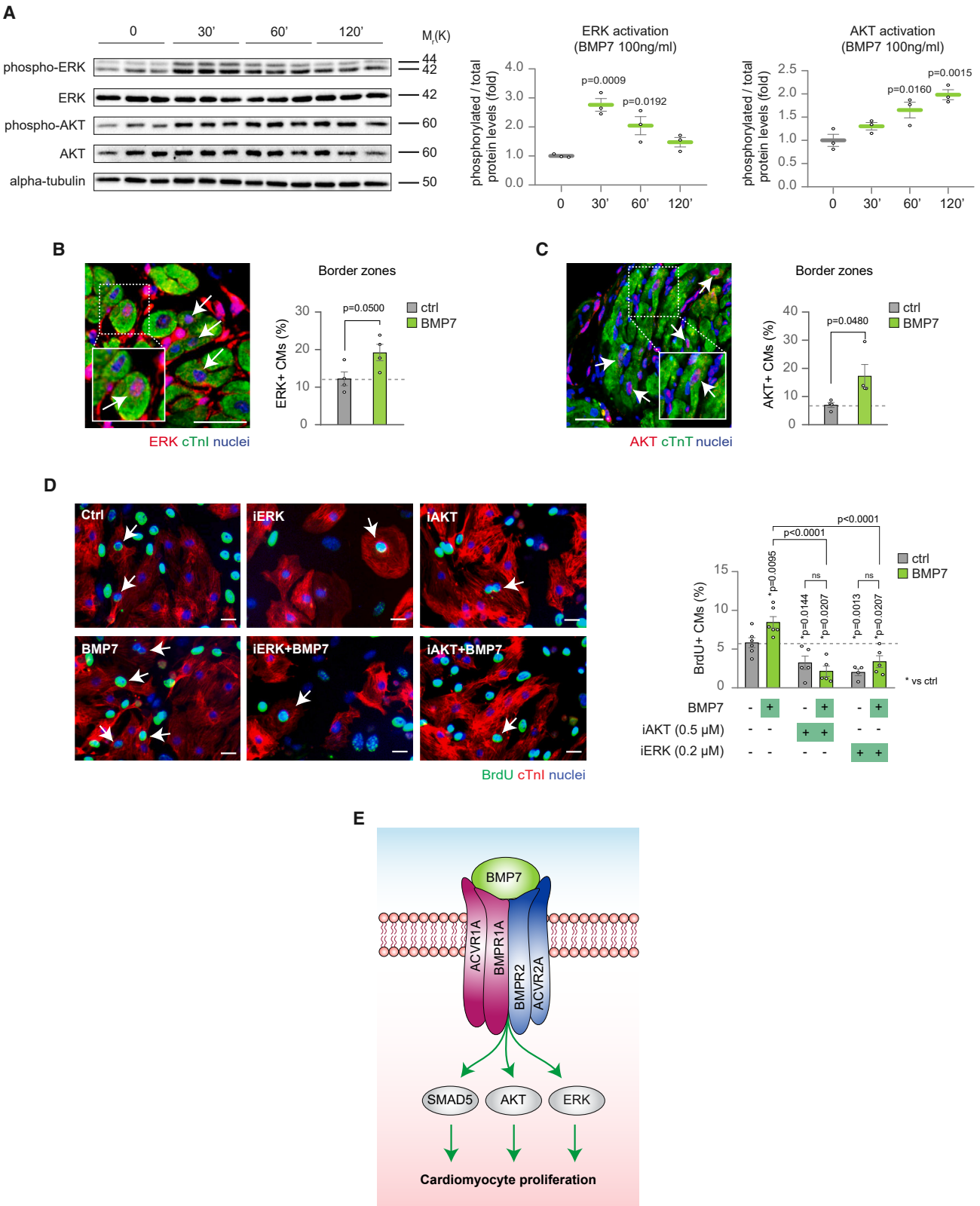

(legend on next page)

proliferate and migrate into the damaged areas after MI,[83–85] our data suggest an additional mechanism for the previously reported anti-fibrotic effect of BMP7 after cardiac injury.[60]

In conclusion, our study supports the concept that a temporal decline in the abundance of specific cardiac growth factors contributes to the exit of cardiomyocytes from the cell cycle and the loss of cardiac regenerative ability in mammals. Among these factors, BMP7, which is predominantly produced by cardiomyocytes in an autocrine manner, appears to be a potent inducer of mammalian cardiomyocyte proliferation both *in vitro* and *in vivo*. BMP7 has a pro-regenerative activity on cardiomyocytes also in the zebrafish model, in which heart regeneration naturally occurs. Therefore, we propose BMP7 delivery as a promising strategy to trigger the regeneration of endogenous cardiomyocytes.

Limitations of the study

Our data show that *in vivo* administration of BMP7 after MI promotes cardiomyocyte regeneration in murine models. While our findings suggest potential therapeutic benefits of BMP7, additional investigations are warranted to assess its effects on other organs following systemic administration. Furthermore, elucidating the optimal timing and delivery methods of BMP7 is crucial for its clinical translation in human patients.

Moreover, our *in vitro* analyses revealed the involvement of the SMAD5, ERK, and AKT pathways in mediating the proliferative effect of BMP7. Although we also documented the activation of these pathways upon BMP7 administration *in vivo* post-MI, further studies involving their genetic manipulation are necessary to validate their functional role in mediating BMP7-induced heart regeneration *in vivo*.

STAR★METHODS

Detailed methods are provided in the online version of this paper and include the following:

SUPPLEMENTAL INFORMATION

Supplemental information can be found online at https://doi.org/10.1016/j.celrep.2024.114162.

ACKNOWLEDGMENTS

The research leading to these results has received funding from the European Union - NextGenerationEU through the Italian Ministry of University and Research under PNRR - M4C2-I1.3 Project PE_00000019 "HEAL ITALIA" to G.D'U. CUP J33C22002920006. The views and opinions expressed are those of the authors only and do not necessarily reflect those of the European Union or the European Commission. Neither the European Union nor the European Commission can be responsible for them. The research was also supported by the European Union's Horizon 2020 research and innovation programme under the ERA-NET on Cardiovascular Diseases (ERA-CVD) Co-fund action to G.D'U., G.W., and E.T. (Grant Number: JCT2016-40-080), by Fondazione Luisa Fanti Melloni to G.D'U., and by the Italian Ministry of Health (RC-2024-2790614). The D'Uva lab extends its gratitude to Milena Pariali for her technical support in sectioning paraffin-embedded samples and to Desirè Zambroni for her technical assistance in *in vitro* immunofluorescence imaging at ALEMBIC, an advanced microscopy laboratory established by IRCCS Ospedale San Raffaele and Università Vita-Salute San Raffaele.

E.T. was supported by the European Research Council (ERC AdG #788194), the European Union's Horizon 2020 research and innovation programme (874764), and the Israel Science Foundation (ISF).

G.W. was supported by the Deutsche Forschungsgemeinschaft (DFG, German Research Foundation) Project-ID 251293561 – SFB 1149 (project C03), project ID 316249678 – SFB 1279 (project Z02), and project ID 450627322 – SFB 1506 (project C04). The Weidinger lab acknowledges the Core facility "light microscopy" of the Medical Faculty of Ulm University for help with imaging.

Figure 7. ERK and AKT non-canonical pathways take part in BMP7 mitogenic signal transduction

(A) Western blot analysis of protein levels of phospho-ERK, ERK, phospho-AKT, AKT, and alpha-tubulin in neonatal (postnatal day 1, P1) cardiac cultures following stimulation with 100 ng/mL BMP7 for 30, 60, and 120 min (n = 3 replicates per condition). Alpha-tubulin protein levels are provided as second loading control.

(B and C) Immunofluorescence analysis for (B) ERK and cardiac Troponin I (cTnI) or (C) AKT and cardiac Troponin T (cTnT) in the border zones of heart sections 14 days post myocardial infarction, following daily injection of BMP7 or water as control (n = 8 mice; a total of 9,318 and 4,652 cardiomyocytes have been analyzed in B and C, respectively). Cardiomyocytes with nuclear ERK or AKT immunoreactivity were counted manually within border zones in tissue sections; every dot represents a different heart (biological replicate), which in turn has been calculated by the analysis of one to two sections. Representative pictures are provided; arrows point at ERK-positive cardiomyocytes in (B) and at AKT-positive cardiomyocytes in (C); scale bars, 20 μm.

(D) Quantification of BrdU incorporation in neonatal (postnatal day 1, P1) cardiomyocytes upon treatment with inhibitors of AKT (Akt inhibitor VIII 0.5 μM) or ERK (PD0325901 0.2 μM), with or without administration of BMP7 at 10 ng/mL for 48 h (n = 8204 cardiomyocytes pooled from the analysis of 31 samples); cardiomyocytes were identified by cardiac Troponin I (cTnI) immunostaining. Representative pictures are provided; arrows point at proliferating cardiomyocytes; scale bars, 20 μm.

(E) BMP7 signal transduction model triggering cardiomyocyte proliferation, showing the involvement of canonical SMAD5 and non-canonical ERK and AKT. The values in (A)–(D) are presented as mean (error bars show SEM), statistical significance was determined using one-way ANOVA followed by Sidak's test in (A) and (D) (comparison between pairs of treatments), and using two-sided Student's t test in (B) and (C).

AUTHOR CONTRIBUTIONS

C.B. and G.D'U. designed the experiments. C.B. carried out most of the experiments and analyzed the data. H.B.L. performed myocardial infarction experiments on mouse models. D.P.P. performed experiments on adult zebrafish. S.R. and M.B. generated and characterized zebrafish transgenic lines and performed cryoinjury experiments in zebrafish models. L.K. cloned zebrafish constructs, and D.P.P. and L.K. performed experiments on zebrafish embryos. I.D.B., S.D.P., F.S., C.M., S.B., F.P., and I.P. performed immunofluorescence, western blots, and gene expression analysis. R.T. helped with immunofluorescence image acquisition and time-lapse imaging. D.R. and M.M. helped with western blot analysis. E.T., G.W., S.H., C.V., and M.L. supervised the experiments done by their laboratory members, and G.D'U. supervised the entire project. C.B. and G.D'U. wrote the manuscript, with editing contributions from all authors.

DECLARATION OF INTERESTS

The authors declare no competing interests.

Received: November 8, 2023
Revised: March 6, 2024
Accepted: April 11, 2024
Published: April 27, 2024

REFERENCES

1. Bongiovanni, C., Sacchi, F., Da Pra, S., Pantano, E., Miano, C., Morelli, M.B., and D'Uva, G. (2021). Reawakening the Intrinsic Cardiac Regenerative Potential: Molecular Strategies to Boost Dedifferentiation and Proliferation of Endogenous Cardiomyocytes. Front. Cardiovasc. Med. *8*, 750604. https://doi.org/10.3389/fcvm.2021.750604.
2. Tzahor, E., and Poss, K.D. (2017). Cardiac regeneration strategies: Staying young at heart. Science *356*, 1035–1039. https://doi.org/10.1126/science.aam5894.
3. Sadek, H., and Olson, E.N. (2020). Toward the Goal of Human Heart Regeneration. Cell Stem Cell *26*, 7–16. https://doi.org/10.1016/j.stem.2019.12.004.
4. Benjamin, E.J., Muntner, P., Alonso, A., Bittencourt, M.S., Callaway, C.W., Carson, A.P., Chamberlain, A.M., Chang, A.R., Cheng, S., Das, S.R., et al. (2019). Heart Disease and Stroke Statistics-2019 Update: A Report from the American Heart Association 10.1161/CIR.0000000000000659.
5. van Berlo, J.H., and Molkentin, J.D. (2014). An emerging consensus on cardiac regeneration. Nat. Med. *20*, 1386–1393. https://doi.org/10.1038/nm.3764.
6. Eschenhagen, T., Bolli, R., Braun, T., Field, L.J., Fleischmann, B.K., Frisén, J., Giacca, M., Hare, J.M., Houser, S., Lee, R.T., et al. (2017). Cardiomyocyte Regeneration: A Consensus Statement. Circulation *136*, 680–686. https://doi.org/10.1161/CIRCULATIONAHA.117.029343.
7. Poss, K.D., Wilson, L.G., and Keating, M.T. (2002). Heart regeneration in zebrafish. Science *298*, 2188–2190. https://doi.org/10.1126/science.1077857.
8. Price, E.L., Vieira, J.M., and Riley, P.R. (2019). Model organisms at the heart of regeneration. Dis. Model. Mech. *12*, dmm040691. https://doi.org/10.1242/dmm.040691.
9. Marques, I.J., Lupi, E., and Mercader, N. (2019). Model systems for regeneration: zebrafish. Development *146*, dev167692. https://doi.org/10.1242/dev.167692.
10. Drenckhahn, J.-D., Schwarz, Q.P., Gray, S., Laskowski, A., Kiriazis, H., Ming, Z., Harvey, R.P., Du, X.-J., Thorburn, D.R., and Cox, T.C. (2008). Compensatory growth of healthy cardiac cells in the presence of diseased cells restores tissue homeostasis during heart development. Dev. Cell *15*, 521–533. https://doi.org/10.1016/j.devcel.2008.09.005.
11. Porrello, E.R., Mahmoud, A.I., Simpson, E., Hill, J.A., Richardson, J.A., Olson, E.N., and Sadek, H.A. (2011). Transient regenerative potential of the neonatal mouse heart. Science *331*, 1078–1080. https://doi.org/10.1126/science.1200708.
12. Bryant, D.M., O'Meara, C.C., Ho, N.N., Gannon, J., Cai, L., and Lee, R.T. (2015). A systematic analysis of neonatal mouse heart regeneration after apical resection. J. Mol. Cell. Cardiol. *79*, 315–318. https://doi.org/10.1016/j.yjmcc.2014.12.011.
13. Sampaio-Pinto, V., Rodrigues, S.C., Laundos, T.L., Silva, E.D., Vasques-Nóvoa, F., Silva, A.C., Cerqueira, R.J., Resende, T.P., Pianca, N., Leite-Moreira, A., et al. (2018). Neonatal Apex Resection Triggers Cardiomyocyte Proliferation, Neovascularization and Functional Recovery Despite Local Fibrosis. Stem Cell Rep. *10*, 860–874. https://doi.org/10.1016/j.stemcr.2018.01.042.
14. Zhu, W., Zhang, E., Zhao, M., Chong, Z., Fan, C., Tang, Y., Hunter, J.D., Borovjagin, A.V., Walcott, G.P., Chen, J.Y., et al. (2018). Regenerative Potential of Neonatal Porcine Hearts. Circulation *138*, 2809–2816. https://doi.org/10.1161/CIRCULATIONAHA.118.034886.
15. Ye, L., D'Agostino, G., Loo, S.J., Wang, C.X., Su, L.P., Tan, S.H., Tee, G.Z., Pua, C.J., Pena, E.M., Cheng, R.B., et al. (2018). Early Regenerative Capacity in the Porcine Heart. Circulation *138*, 2798–2808. https://doi.org/10.1161/CIRCULATIONAHA.117.031542.
16. Haubner, B.J., Adamowicz-Brice, M., Khadayate, S., Tiefenthaler, V., Metzler, B., Aitman, T., and Penninger, J.M. (2012). Complete cardiac regeneration in a mouse model of myocardial infarction. Aging (Albany. NY) *4*, 966–977. https://doi.org/10.18632/aging.100526.
17. Li, F., Wang, X., Capasso, J.M., and Gerdes, A.M. (1996). Rapid transition of cardiac myocytes from hyperplasia to hypertrophy during postnatal development. J. Mol. Cell. Cardiol. *28*, 1737–1746. https://doi.org/10.1006/jmcc.1996.0163.
18. Soonpaa, M.H., and Field, L.J. (1998). Survey of studies examining mammalian cardiomyocyte DNA synthesis. Circ. Res. *83*, 15–26. https://doi.org/10.1016/S1566-0702(01)00339-3.
19. Bergmann, O., Bhardwaj, R.D., Bernard, S., Zdunek, S., Barnabé-Heider, F., Walsh, S., Zupicich, J., Alkass, K., Buchholz, B.A., Druid, H., et al. (2009). Evidence for cardiomyocyte renewal in humans. Science *324*, 98–102. https://doi.org/10.1126/science.1164680.
20. Senyo, S.E., Steinhauser, M.L., Pizzimenti, C.L., Yang, V.K., Cai, L., Wang, M., Wu, T.D., Guerquin-Kern, J.L., Lechene, C.P., and Lee, R.T. (2013). Mammalian heart renewal by pre-existing cardiomyocytes. Nature *493*, 433–436. https://doi.org/10.1038/nature11682nature11682.
21. Jopling, C., Sleep, E., Raya, M., Martí, M., Raya, A., Izpisúa Belmonte, J.C., and Izpisúa Belmonte, J.C. (2010). Zebrafish heart regeneration occurs by cardiomyocyte dedifferentiation and proliferation. Nature *464*, 606–609. https://doi.org/10.1038/nature08899.
22. Kikuchi, K., Holdway, J.E., Werdich, A.A., Anderson, R.M., Fang, Y., Egnaczyk, G.F., Evans, T., Macrae, C. a, Stainier, D.Y.R., and Poss, K.D. (2010). Primary contribution to zebrafish heart regeneration by gata4(+) cardiomyocytes. Nature *464*, 601–605. https://doi.org/10.1038/nature08804.
23. Bersell, K., Arab, S., Haring, B., and Kühn, B. (2009). Neuregulin1/ErbB4 signaling induces cardiomyocyte proliferation and repair of heart injury. Cell *138*, 257–270. https://doi.org/10.1016/j.cell.2009.04.060S0092-8674(09)00522-4.
24. D'Uva, G., Aharonov, A., Lauriola, M., Kain, D., Yahalom-Ronen, Y., Carvalho, S., Weisinger, K., Bassat, E., Rajchman, D., Yifa, O., et al. (2015). ERBB2 triggers mammalian heart regeneration by promoting cardiomyocyte dedifferentiation and proliferation. Nat. Cell Biol. *17*, 627–638. https://doi.org/10.1038/ncb3149.
25. Engel, F.B., Hsieh, P.C.H., Lee, R.T., and Keating, M.T. (2006). FGF1/p38 MAP kinase inhibitor therapy induces cardiomyocyte mitosis, reduces scarring, and rescues function after myocardial infarction. Proc. Natl. Acad. Sci. USA *103*, 15546–15551. https://doi.org/10.1073/pnas.0607382103.

26. Sun, L., Yu, J., Qi, S., Hao, Y., Liu, Y., and Li, Z. (2014). Bone Morphogenetic Protein-10 Induces Cardiomyocyte Proliferation and Improves Cardiac Function after Myocardial Infarction. J. Cell. Biochem. *115*, 1868–1876. https://doi.org/10.1002/jcb.24856.

27. Kubin, T., Pöling, J., Kostin, S., Gajawada, P., Hein, S., Rees, W., Wietelmann, A., Tanaka, M., Lörchner, H., Schimanski, S., et al. (2011). Oncostatin M is a major mediator of cardiomyocyte dedifferentiation and remodeling. Cell Stem Cell *9*, 420–432. https://doi.org/10.1016/j.stem.2011.08.013.

28. Li, Y., Feng, J., Song, S., Li, H., Yang, H., Zhou, B., Li, Y., Yue, Z., Lian, H., Liu, L., et al. (2020). gp130 Controls Cardiomyocyte Proliferation and Heart Regeneration. Circulation *142*, 967–982. https://doi.org/10.1161/CIRCULATIONAHA.119.044484.

29. Novoyatleva, T., Diehl, F., van Amerongen, M.J., Patra, C., Ferrazzi, F., Bellazzi, R., and Engel, F.B. (2010). TWEAK is a positive regulator of cardiomyocyte proliferation. Cardiovasc. Res. *85*, 681–690. https://doi.org/10.1093/cvr/cvp360.

30. Zacchigna, S., Martinelli, V., Moimas, S., Colliva, A., Anzini, M., Nordio, A., Costa, A., Rehman, M., Vodret, S., Pierro, C., et al. (2018). Paracrine effect of regulatory T cells promotes cardiomyocyte proliferation during pregnancy and after myocardial infarction. Nat. Commun. *9*, 2432. https://doi.org/10.1038/s41467-018-04908-z.

31. Wei, K., Serpooshan, V., Hurtado, C., Diez-Cuñado, M., Zhao, M., Maruyama, S., Zhu, W., Fajardo, G., Noseda, M., Nakamura, K., et al. (2015). Epicardial FSTL1 reconstitution regenerates the adult mammalian heart. Nature *525*, 479–485. https://doi.org/10.1038/nature15372.

32. Tao, Z., Chen, B., Tan, X., Zhao, Y., Wang, L., Zhu, T., Cao, K., Yang, Z., Kan, Y.W., and Su, H. (2011). Coexpression of VEGF and angiopoietin-1 promotes angiogenesis and cardiomyocyte proliferation reduces apoptosis in porcine myocardial infarction (MI) heart. Proc. Natl. Acad. Sci. USA *108*, 2064–2069. https://doi.org/10.1073/pnas.1018925108.

33. Vukicevic, S., Colliva, A., Kufner, V., Martinelli, V., Moimas, S., Vodret, S., Rumenovic, V., Milosevic, M., Brkljacic, B., Delic-Brkljacic, D., et al. (2022). Bone morphogenetic protein 1.3 inhibition decreases scar formation and supports cardiomyocyte survival after myocardial infarction. Nat. Commun. *13*, 81. https://doi.org/10.1038/s41467-021-27622-9.

34. Chakraborty, S., Sengupta, A., and Yutzey, K.E. (2013). Tbx20 promotes cardiomyocyte proliferation and persistence of fetal characteristics in adult mouse hearts. J. Mol. Cell. Cardiol. *62*, 203–213. https://doi.org/10.1016/j.yjmcc.2013.05.018.

35. Ebelt, H., Hillebrand, I., Arlt, S., Zhang, Y., Kostin, S., Neuhaus, H., Müller-Werdan, U., Schwarz, E., Werdan, K., and Braun, T. (2013). Treatment with bone morphogenetic protein 2 limits infarct size after myocardial infarction in mice. Shock *39*, 353–360. https://doi.org/10.1097/SHK.0b013e318289728a.

36. Hirose, K., Payumo, A.Y., Cutie, S., Hoang, A., Zhang, H., Guyot, R., Lunn, D., Bigley, R.B., Yu, H., Wang, J., et al. (2019). Evidence for hormonal control of heart regenerative capacity during endothermy acquisition. Science *364*, 184–188. https://doi.org/10.1126/science.aar2038.

37. Pianca, N., Sacchi, F., Umansky, K.B., Chirivì, M., Iommarini, L., Da Pra, S., Papa, V., Bongiovanni, C., Miano, C., Pontis, F., et al. (2022). Glucocorticoid receptor antagonization propels endogenous cardiomyocyte proliferation and cardiac regeneration. Nat. Cardiovasc. Res. *1*, 617–633. https://doi.org/10.1038/s44161-022-00090-0.

38. Garbern, J.C., and Lee, R.T. (2022). Heart regeneration: 20 years of progress and renewed optimism. Dev. Cell *57*, 424–439. https://doi.org/10.1016/j.devcel.2022.01.012.

39. Galdos, F.X., Guo, Y., Paige, S.L., VanDusen, N.J., Wu, S.M., and Pu, W.T. (2017). Cardiac Regeneration: Lessons From Development. Circ. Res. *120*, 941–959. https://doi.org/10.1161/CIRCRESAHA.116.309040.

40. Uygur, A., and Lee, R.T. (2016). Mechanisms of Cardiac Regeneration. Dev. Cell *36*, 362–374. https://doi.org/10.1016/j.devcel.2016.01.018.

41. Heallen, T.R., Kadow, Z.A., Kim, J.H., Wang, J., and Martin, J.F. (2019). Stimulating Cardiogenesis as a Treatment for Heart Failure. Circ. Res. *124*, 1647–1657. https://doi.org/10.1161/CIRCRESAHA.118.313573.

42. Hashimoto, H., Olson, E.N., and Bassel-Duby, R. (2018). Therapeutic approaches for cardiac regeneration and repair. Nat. Rev. Cardiol. *15*, 585–600. https://doi.org/10.1038/s41569-018-0036-6.

43. Cahill, T.J., Choudhury, R.P., and Riley, P.R. (2017). Heart regeneration and repair after myocardial infarction: translational opportunities for novel therapeutics. Nat. Rev. Drug Discov. *16*, 699–717. https://doi.org/10.1038/nrd.2017.106.

44. Talman, V., Teppo, J., Pöhö, P., Movahedi, P., Vaikkinen, A., Karhu, S.T., Trošt, K., Suvitaival, T., Heikkonen, J., Pahikkala, T., et al. (2018). Molecular Atlas of Postnatal Mouse Heart Development. J. Am. Heart Assoc. *7*, e010378. https://doi.org/10.1161/JAHA.118.010378.

45. Hashimoto, H., Yuasa, S., Tabata, H., Tohyama, S., Hayashiji, N., Hattori, F., Muraoka, N., Egashira, T., Okata, S., Yae, K., et al. (2014). Time-lapse imaging of cell cycle dynamics during development in living cardiomyocyte. J. Mol. Cell. Cardiol. *72*, 241–249. https://doi.org/10.1016/j.yjmcc.2014.03.020.

46. Polizzotti, B.D., Ganapathy, B., Walsh, S., Choudhury, S., Ammanamanchi, N., Bennett, D.G., Dos Remedios, C.G., Haubner, B.J., Penninger, J.M., Kühn, B., et al. (2015). Neuregulin stimulation of cardiomyocyte regeneration in mice and human myocardium reveals a therapeutic window. Sci. Transl. Med. *7*, 281ra45. https://doi.org/10.1126/scitranslmed.aaa5171.

47. Zacchigna, S., Martinelli, V., Moimas, S., Colliva, A., Anzini, M., Nordio, A., Costa, A., Rehman, M., Vodret, S., Pierro, C., et al. (2018). Paracrine effect of regulatory T cells promotes cardiomyocyte proliferation during pregnancy and after myocardial infarction. Nat. Commun. *9*, 2432–2512. https://doi.org/10.1038/s41467-018-04908-z.

48. Shen, H., Gan, P., Wang, K., Darehzereshki, A., Wang, K., Kumar, S.R., Lien, C.-L., Patterson, M., Tao, G., and Sucov, H.M. (2020). Mononuclear diploid cardiomyocytes support neonatal mouse heart regeneration in response to paracrine IGF2 signaling. Elife *9*, e53071. https://doi.org/10.7554/eLife.53071.

49. Tang, P., Ma, S., Dong, M., Wang, J., Chai, S., Liu, T., and Li, J. (2018). Effect of interleukin-6 on myocardial regeneration in mice after cardiac injury. Biomed. Pharmacother. *106*, 303–308. https://doi.org/10.1016/j.biopha.2018.06.090.

50. Palmer, J.N., Hartogensis, W.E., Patten, M., Fortuin, F.D., and Long, C.S. (1995). Interleukin-1 beta induces cardiac myocyte growth but inhibits cardiac fibroblast proliferation in culture. J. Clin. Invest. *95*, 2555–2564. https://doi.org/10.1172/JCI117956.

51. Li, Z., Hu, S., Huang, K., Su, T., Cores, J., and Cheng, K. (2020). Targeted anti-IL-1β platelet microparticles for cardiac detoxing and repair. Sci. Adv. *6*, eaay0589. https://doi.org/10.1126/sciadv.aay0589.

52. Soonpaa, M.H., Kim, K.K., Pajak, L., Franklin, M., and Field, L.J. (1996). Cardiomyocyte DNA synthesis and binucleation during murine development. Am. J. Physiol. *271*, H2183–H2189.

53. Derks, W., and Bergmann, O. (2020). Polyploidy in Cardiomyocytes: Roadblock to Heart Regeneration? Circ. Res. *126*, 552–565. https://doi.org/10.1161/CIRCRESAHA.119.315408.

54. Hattori, F., Chen, H., Yamashita, H., Tohyama, S., Satoh, Y.-S., Yuasa, S., Li, W., Yamakawa, H., Tanaka, T., Onitsuka, T., et al. (2010). Nongenetic method for purifying stem cell-derived cardiomyocytes. Nat. Methods *7*, 61–66. https://doi.org/10.1038/nmeth.1403.

55. Shawi, M., and Serluca, F.C. (2008). Identification of a BMP7 homolog in zebrafish expressed in developing organ systems. Gene Expr. Patterns *8*, 369–375. https://doi.org/10.1016/j.gep.2008.05.004.

56. Dong, X.-R., Wan, S.-M., Zhou, J.-J., Nie, C.-H., Chen, Y.-L., Diao, J.-H., and Gao, Z.-X. (2022). Functional Differentiation of BMP7 Genes in Zebrafish: bmp7a for Dorsal-Ventral Pattern and bmp7b for Melanin Synthesis

and Eye Development. Front. Cell Dev. Biol. *10*, 838721. https://doi.org/10.3389/fcell.2022.838721.

57. Wu, C.-C., Kruse, F., Vasudevarao, M.D., Junker, J.P., Zebrowski, D.C., Fischer, K., Noël, E.S., Grün, D., Berezikov, E., Engel, F.B., et al. (2016). Spatially Resolved Genome-wide Transcriptional Profiling Identifies BMP Signaling as Essential Regulator of Zebrafish Cardiomyocyte Regeneration. Dev. Cell *36*, 36–49. https://doi.org/10.1016/j.devcel.2015.12.010.
58. Schmid, B., Fürthauer, M., Connors, S.A., Trout, J., Thisse, B., Thisse, C., and Mullins, M.C. (2000). Equivalent genetic roles for bmp7/snailhouse and bmp2b/swirl in dorsoventral pattern formation. Development *127*, 957–967. https://doi.org/10.1242/dev.127.5.957.
59. Quaife-Ryan, G.A., Sim, C.B., Ziemann, M., Kaspi, A., Rafehi, H., Ramialison, M., El-Osta, A., Hudson, J.E., and Porrello, E.R. (2017). Multi-Cellular Transcriptional Analysis of Mammalian Heart Regeneration. Circulation *136*, 1123–1139. https://doi.org/10.1161/CIRCULATIONAHA.117.028252.
60. Jin, Y., Cheng, X., Lu, J., and Li, X. (2018). Exogenous BMP-7 Facilitates the Recovery of Cardiac Function after Acute Myocardial Infarction through Counteracting TGF-β1 Signaling Pathway. Tohoku J. Exp. Med. *244*, 1–6. https://doi.org/10.1620/tjem.244.1.
61. Miyazono, K., Maeda, S., and Imamura, T. (2005). BMP receptor signaling: Transcriptional targets, regulation of signals, and signaling cross-talk. Cytokine Growth Factor Rev. *16*, 251–263. https://doi.org/10.1016/j.cytogfr.2005.01.009.
62. Heldin, C.-H., and Moustakas, A. (2016). Signaling Receptors for TGF-β Family Members. Cold Spring Harb. Perspect. Biol. *8*, a022053. https://doi.org/10.1101/cshperspect.a022053.
63. Loomans, H.A., and Andl, C.D. (2016). Activin receptor-like kinases: A diverse family playing an important role in cancer. Am. J. Cancer Res. *6*, 2431–2447.
64. Lavery, K., Swain, P., Falb, D., and Alaoui-Ismaili, M.H. (2008). BMP-2/4 and BMP-6/7 differentially utilize cell surface receptors to induce osteoblastic differentiation of human bone marrow-derived mesenchymal stem cells. J. Biol. Chem. *283*, 20948–20958. https://doi.org/10.1074/jbc.M800850200.
65. González-Gómez, P., Crecente-Campo, J., Zahonero, C., de la Fuente, M., Hernández-Laín, A., Mira, H., Sánchez-Gómez, P., and Garcia-Fuentes, M. (2015). Controlled release microspheres loaded with BMP7 suppress primary tumors from human glioblastoma. Oncotarget *6*, 10950–10963. https://doi.org/10.18632/oncotarget.3459.
66. Yamashita, H., ten Dijke, P., Huylebroeck, D., Sampath, T.K., Andries, M., Smith, J.C., Heldin, C.H., and Miyazono, K. (1995). Osteogenic protein-1 binds to activin type II receptors and induces certain activin-like effects. J. Cell Biol. *130*, 217–226. https://doi.org/10.1083/jcb.130.1.217.
67. Massagué, J., Seoane, J., and Wotton, D. (2005). Smad transcription factors. Genes Dev. *19*, 2783–2810. https://doi.org/10.1101/gad.1350705.
68. Zhang, Y.E. (2017). Non-Smad signaling pathways of the TGF-β family. Cold Spring Harb. Perspect. Biol. *9*, a022129. https://doi.org/10.1101/cshperspect.a022129.
69. Elmadbouh, I., and Singla, D.K. (2021). BMP-7 Attenuates Inflammation-Induced Pyroptosis and Improves Cardiac Repair in Diabetic Cardiomyopathy. Cells *10*, 2640. https://doi.org/10.3390/cells10102640.
70. Tate, M., Perera, N., Prakoso, D., Willis, A.M., Deo, M., Oseghale, O., Qian, H., Donner, D.G., Kiriazis, H., De Blasio, M.J., et al. (2021). Bone Morphogenetic Protein 7 Gene Delivery Improves Cardiac Structure and Function in a Murine Model of Diabetic Cardiomyopathy. Front. Pharmacol. *12*, 719290. https://doi.org/10.3389/fphar.2021.719290.
71. Zeisberg, E.M., Tarnavski, O., Zeisberg, M., Dorfman, A.L., McMullen, J.R., Gustafsson, E., Chandraker, A., Yuan, X., Pu, W.T., Roberts, A.B., et al. (2007). Endothelial-to-mesenchymal transition contributes to cardiac fibrosis. Nat. Med. *13*, 952–961. https://doi.org/10.1038/nm1613.
72. Merino, D., Villar, A.V., García, R., Tramullas, M., Ruiz, L., Ribas, C., Cabezudo, S., Nistal, J.F., and Hurlé, M.A. (2016). BMP-7 attenuates left ventricular remodelling under pressure overload and facilitates reverse remodelling and functional recovery. Cardiovasc. Res. *110*, 331–345. https://doi.org/10.1093/cvr/cvw076.
73. Salido-Medina, A.B., Gil, A., Expósito, V., Martínez, F., Redondo, J.M., Hurlé, M.A., Nistal, J.F., and García, R. (2022). BMP7-based peptide agonists of BMPR1A protect the left ventricle against pathological remodeling induced by pressure overload. Biomed. Pharmacother. *149*, 112910. https://doi.org/10.1016/j.biopha.2022.112910.
74. D'Uva, G., and Tzahor, E. (2015). The key roles of ERBB2 in cardiac regeneration. Cell Cycle *14*, 2383–2384. https://doi.org/10.1080/15384101.2015.1063292.
75. Tan, C.Y., Wong, J.X., Chan, P.S., Tan, H., Liao, D., Chen, W., Tan, L.W., Ackers-Johnson, M., Wakimoto, H., Seidman, J.G., et al. (2019). Yin Yang 1 Suppresses Dilated Cardiomyopathy and Cardiac Fibrosis Through Regulation of Bmp7 and Ctgf. Circ. Res. *125*, 834–846. https://doi.org/10.1161/CIRCRESAHA.119.314794.
76. Cao, Y., Wang, Y., Zhou, Z., Pan, C., Jiang, L., Zhou, Z., Meng, Y., Charugundla, S., Li, T., Allayee, H., et al. (2022). Liver-heart cross-talk mediated by coagulation factor XI protects against heart failure. Science *377*, 1399–1406. https://doi.org/10.1126/science.abn0910.
77. Aluganti Narasimhulu, C., and Singla, D.K. (2020). The Role of Bone Morphogenetic Protein 7 (BMP-7) in Inflammation in Heart Diseases. Cells *9*, 280–330. https://doi.org/10.3390/cells9020280.
78. Weiskirchen, R., Meurer, S.K., Gressner, O.A., Herrmann, J., Borkham-Kamphorst, E., and Gressner, A.M. (2009). BMP-7 as antagonist of organ fibrosis. Front. Biosci. *14*, 4992–5012. https://doi.org/10.2741/3583.
79. Chen, X., Xu, J., Jiang, B., and Liu, D. (2016). Bone Morphogenetic Protein-7 Antagonizes Myocardial Fibrosis Induced by Atrial Fibrillation by Restraining Transforming Growth Factor-β (TGF-β)/Smads Signaling. Med. Sci. Monit. *22*, 3457–3468. https://doi.org/10.12659/msm.897560.
80. Zaidi, S.H.E., Huang, Q., Momen, A., Riazi, A., and Husain, M. (2010). Growth differentiation factor 5 regulates cardiac repair after myocardial infarction. J. Am. Coll. Cardiol. *55*, 135–143. https://doi.org/10.1016/j.jacc.2009.08.041.
81. Izumi, M., Fujio, Y., Kunisada, K., Negoro, S., Tone, E., Funamoto, M., Osugi, T., Oshima, Y., Nakaoka, Y., Kishimoto, T., et al. (2001). Bone morphogenetic protein-2 inhibits serum deprivation-induced apoptosis of neonatal cardiac myocytes through activation of the Smad1 pathway. J. Biol. Chem. *276*, 31133–31141. https://doi.org/10.1074/jbc.M101463200.
82. Sun, Y., Fu, J., Xue, X., Yang, H., and Wu, L. (2018). BMP7 regulates lung fibroblast proliferation in newborn rats with bronchopulmonary dysplasia. Mol. Med. Rep. *17*, 6277–6284. https://doi.org/10.3892/mmr.2018.8692.
83. Fu, X., Khalil, H., Kanisicak, O., Boyer, J.G., Vagnozzi, R.J., Maliken, B.D., Sargent, M.A., Prasad, V., Valiente-Alandi, I., Blaxall, B.C., and Molkentin, J.D. (2018). Specialized fibroblast differentiated states underlie scar formation in the infarcted mouse heart. J. Clin. Invest. *128*, 2127–2143. https://doi.org/10.1172/JCI98215.
84. Le Bras, A. (2018). Dynamics of fibroblast activation in the infarcted heart. Nat. Rev. Cardiol. *15*, 379. https://doi.org/10.1038/s41569-018-0025-9.
85. Eschenhagen, T. (2018). A new concept of fibroblast dynamics in post-myocardial infarction remodeling. J. Clin. Invest. *128*, 1731–1733. https://doi.org/10.1172/JCI121079.
86. Kwan, K.M., Fujimoto, E., Grabher, C., Mangum, B.D., Hardy, M.E., Campbell, D.S., Parant, J.M., Yost, H.J., Kanki, J.P., and Chien, C.-B. (2007). The Tol2kit: a multisite gateway-based construction kit for Tol2 transposon transgenesis constructs. Dev. Dyn. *236*, 3088–3099. https://doi.org/10.1002/dvdy.21343.
87. Pianca, N., Di Bona, A., Lazzeri, E., Costantini, I., Franzoso, M., Prando, V., Armani, A., Rizzo, S., Fedrigo, M., Angelini, A., et al. (2019). Cardiac sympathetic innervation network shapes the myocardium by locally controlling cardiomyocyte size through the cellular proteolytic machinery. J. Physiol. *597*, 3639–3656. https://doi.org/10.1113/JP276200.

88. Omatsu-Kanbe, M., Yoshioka, K., Fukunaga, R., Sagawa, H., and Matsuura, H. (2018). A simple antegrade perfusion method for isolating viable single cardiomyocytes from neonatal to aged mice. Physiol. Rep. *6*, e13688. https://doi.org/10.14814/phy2.13688.

89. Engel, F.B., Schebesta, M., Duong, M.T., Lu, G., Ren, S., Madwed, J.B., Jiang, H., Wang, Y., and Keating, M.T. (2005). p38 MAP kinase inhibition enables proliferation of adult mammalian cardiomyocytes. Genes Dev. *19*, 1175–1187. https://doi.org/10.1101/gad.1306705.

90. Wodsedalek, D.J., Paddock, S.J., Wan, T.C., Auchampach, J.A., Kenarsary, A., Tsaih, S.-W., Flister, M.J., and O'Meara, C.C. (2019). IL-13 promotes in vivo neonatal cardiomyocyte cell cycle activity and heart regeneration. Am. J. Physiol. Heart Circ. Physiol. *316*, H24–H34. https://doi.org/10.1152/ajpheart.00521.2018.

91. Kishimoto, Y., Lee, K.H., Zon, L., Hammerschmidt, M., and Schulte-Merker, S. (1997). The molecular nature of zebrafish swirl: BMP2 function is essential during early dorsoventral patterning. Development *124*, 4457–4466. https://doi.org/10.1242/dev.124.22.4457.

92. Schnabel, K., Wu, C.C., Kurth, T., and Weidinger, G. (2011). Regeneration of cryoinjury induced necrotic heart lesions in zebrafish is associated with epicardial activation and cardiomyocyte proliferation. PLoS One *6*, e18503. https://doi.org/10.1371/journal.pone.0018503.

STAR★METHODS

KEY RESOURCES TABLE

REAGENT or RESOURCE	SOURCE	IDENTIFIER
Antibodies		
Mouse monoclonal anti-cardiac Troponin T antibody	Abcam	Cat# ab33589, RRID:AB_727035
Rabbit polyclonal anti- cardiac Troponin I antibody	Abcam	Cat# ab47003, RRID:AB_869982
Rabbit recombinant monoclonal anti-Ki67 antibody	Abcam	Cat# ab16667, RRID:AB_302459
Mouse monoclonal anti-BrdU antibody	DSHB	Cat# G3G4, RRID:AB_1157913
Mouse monoclonal anti-AIM1 (Aurora B) antibody	BD Biosciences	Cat# 611082, RRID:AB_2227708
Rabbit monoclonal anti-Phospho-Smad1 (Ser463/465)/Smad5 (Ser463/465)/Smad9 (Ser465/467) antibody	Cell Signaling Technology	Cat# 13820, RRID:AB_2493181
Mouse monoclonal anti-ERK2 (D-2) antibody	Santa Cruz Biotechnology	Cat# sc-1647, RRID:AB_627547
Rabbit monoclonal anti-Smad1 (D59D7) XP antibody	Cell Signaling Technology	Cat# 6944, RRID:AB_10858882
Rabbit polyclonal anti-Akt antibody	Cell Signaling Technology	Cat# 9272, RRID:AB_329827
Rabbit polyclonal anti-Phospho-Akt (Ser473) antibody	Cell Signaling Technology	Cat# 9271, RRID:AB_329825
Rabbit monoclonal anti-GAPDH antibody	Cell Signaling Technology	Cat# 2118, RRID:AB_561053
Mouse monoclonal anti-ERK-1/ERK-2, diphospho antibody	Sigma-Aldrich	Cat# M8159, RRID:AB_477245
Mouse monoclonal anti-alpha-Tubulin antibody	Sigma-Aldrich	Cat# T5168, RRID:AB_477579
Mouse monoclonal anti-Proliferating Cell Nuclear Antigen antibody	Dako	Cat# M0879, RRID:AB_2160651
Mouse monoclonal anti-MF20 (which detects sarcomeric Myosin heavy chain – MHC)	Developmental Studies Hybridoma Bank	Cat# MF20, RRID:AB_2147781
Rabbit polyclonal anti-Myl7 antibody	GeneTex	Cat# GTX128346, RRID:AB_2885759
Alexa Fluor 488-AffiniPure Goat-Anti-Mouse IgG (H + L)	Jackson ImmunoResearch Labs	Cat# 115-545-003, RRID:AB_2338840
Alexa Fluor 488-AffiniPure Goat-Anti-Rabbit IgG (H + L)	Jackson ImmunoResearch Labs	Cat# 111-545-003, RRID:AB_2338046
Cy3-AffiniPure Goat-Anti-Mouse IgG (H + L)	Jackson ImmunoResearch Labs	Cat# 115-165-003, RRID:AB_2338680
Alexa Fluor 594-AffiniPure Goat-Anti-Rabbit IgG (H + L)	Jackson ImmunoResearch Labs	Cat# 111-585-003, RRID:AB_2338059
Cy3-AffiniPure Goat-Anti-Rabbit IgG (H + L)	Jackson ImmunoResearch Labs	Cat# 111-165-003, RRID:AB_2338000
Anti-rabbit horseradish peroxidase-labelled secondary antibody (Dako EnVision+ System- HRP Labeled Polymer)	Agilent	Cat# K4003; RRID:AB_2630375
Anti-mouse horseradish peroxidase-labelled secondary antibody (Dako EnVision+ System- HRP Labeled Polymer)	Agilent	Cat# K4001; RRID:AB_2827819
Goat anti-Rabbit IgG (H + L) Highly Cross-Adsorbed Secondary Antibody, Alexa Fluor™ 488	Invitrogen	Cat# A11034 RRID:AB_2576217

(*Continued on next page*)

Continued

REAGENT or RESOURCE	SOURCE	IDENTIFIER
Goat anti-Rabbit IgG (H + L) Highly Cross-Adsorbed Secondary Antibody, Alexa Fluor™ 555	Invitrogen	Cat# A21429 RRID:AB_2535850
Goat anti-Mouse IgG (H + L) Highly Cross-Adsorbed Secondary Antibody, Alexa Fluor™ 633	Invitrogen	Cat# A21052 RRID:AB_2535719
Goat anti-Mouse IgG (H + L) Highly Cross-Adsorbed Secondary Antibody, Alexa Fluor 555	Invitrogen	Cat# A21424 RRID:AB_141780
Chemicals, peptides, and recombinant proteins		
Recombinant human Artemin	ImmunoTools	Cat#11343772
Recombinant Human Connective Tissue Growth Factor	ImmunoTools	Cat# 11343480
Recombinant Human B-type Natriuretic Peptide	ImmunoTools	Cat#11343782
Recombinant Human Interleukin-23A/IL-12Bp40	ImmunoTools	Cat#11340232
Recombinant Human Glial-derived Neutrophic Factor	ImmunoTools	Cat#11343792
Recombinant Human Fibroblast Growth Factor 23	ImmunoTools	Cat#11344890
Recombinant Human Interleukin-17F	ImmunoTools	Cat#11349170
Recombinant Human Galectin-3	ImmunoTools	Cat#11344243
Recombinant Human Neuregulin-1b	ImmunoTools	Cat#11343043
Recombinant Human Interleukin-1 beta	ImmunoTools	Cat#11340012
Recombinant Human IGF Binding Protein-1	ImmunoTools	Cat#11343800
Recombinant Human Interleukin-10	ImmunoTools	Cat#11340102
Recombinant Human C-X-C motif chemokine ligand 14	ImmunoTools	Cat#11345190
Recombinant Human Interleukin-17B	ImmunoTools	Cat#11345170
Recombinant Human Interleukin-1 Receptor Antagonist	ImmunoTools	Cat#11344874
Recombinant Human Interleukin-6	ImmunoTools	Cat#11340060
Recombinant Human Insulin-Like Growth Factor-II	ImmunoTools	Cat#11343573
Recombinant Human Macrophage Inflammatory Protein-1 alpha	ImmunoTools	Cat#11343200
Recombinant Human Galectin-7 His tagged	ImmunoTools	Cat#11345240
Recombinant Human Granulocyte Colony Stimulating Factor	ImmunoTools	Cat#11343132
Recombinant Human Bone Morphogenetic protein7 CHO	ImmunoTools	Cat#11343295
Recombinant Human Bone Morphogenetic protein 7	Peprotech	Cat#120-03P
Recombinant Human soluble RANK Ligand	ImmunoTools	Cat# 11343452
Recombinant Human C-X-C motif chemokine ligand 17	ImmunoTools	Cat#11345200
5-Bromo-2′-Deoxyuridine	Sigma-Aldrich	B5002; CAS: RN 59-14-3
Tetramethylrhodamine ethyl ester perchlorate	Sigma-Aldrich	87917; CAS:115532-52-0
Akt Inhibitor VIII, Isozyme-Selective, Akti-1/2	Sigma-Aldrich	124018; CAS:612847-09-3

(*Continued on next page*)

Continued

REAGENT or RESOURCE	SOURCE	IDENTIFIER
ERK inhibitor PD 0325901	Sigma-Aldrich	PZ0162; CAS: 391210-10-9
Pancreatin	Sigma-Aldrich	P1750; CAS: 8049-47-6
Collagenase A	Roche	10103586001; CAS: 9001-12-1
Trypsin	Sigma-Aldrich	T8003; CAS: 9002-07-7
Protease from streptomyces	Sigma-Aldrich	P5147; CAS: 9036-06-0
DAPI (4′,6-diamidino-2-phenylindole dihydrochloride)	Sigma-Aldrich	D9542; CAS:28718-90-3
Proteinase inhibitor	Sigma-Aldrich	P8340; CAS: 30827-99-7
Phosphatase inhibitor (Sodium orthovanadate)	Sigma-Aldrich	450243; CAS: 13721-39-6
Phosphatase inhibitor (Sodium fluoride)	Sigma-Aldrich	CAS: 7681-49-4
Nitrocellulose membrane (AmershamTM ProtranTM Premium 0.45 μm 300 mm × 4 m)	Sigma-Aldrich	GE10600002
Gelatin	Sigma-Aldrich	G9391; CAS: 9000-70-8
Critical commercial assays		
ClickTech EdU Cell Proliferation Kit 647	Baseclick	BCK-EdU647IM100+IV-S
mMessage mMachine kit	Invitrogen	AM1348
RNeasy Fibrous tissue kit	Qiagen	74704
NucleoSpin RNA II kit	Macherey Nagel	FC140955N
SuperScript™ VILO™ cDNA Synthesis Kit	Invitrogen	11754050
Fast SYBR Green PCR Master Mix	Applied Biosystems	4309155
Lipofectamine™ 3000 Transfection Reagent	Thermofisher	L3000008
MACS Neonatal Isolation System	Miltenyi biotech	130-100-825
KASP Master mix	LGC Biosearch Technology	KBS-1050-101
Deposited data		
Raw data from all charts and western blot images	This paper (deposited on Mendeley Data)	https://doi.org/10.17632/8w43fgzdjx.1
RNA-sequencing data analyzed in this study	Talman et al.[44]	GEO: GSE119530
RNA-sequencing data analyzed in this study	Quaife-Ryan et al.[59]	GEO: GSE95764
RNA-sequencing data analyzed in this study	Haubner et al.[16]	Supplemental information
Experimental models: Organisms/strains		
Mice: strain C57BL/6N	Charles River Laboratory	Strain C57BL/6N
Mice: strain C57BL/6JRccHsd	Harlan	Strain C57BL/6JRccHsd
Zebrafish: *hsp70L*:bmp7b, *myl7*:eGFP^{af5Tg}	Stephan Heermann lab (this paper)	N/A
Zebrafish: *bmp7a*$^{ty68a/ty68a}$	Schmid et al.[58]	ZDB-ALT-980203-1308
Oligonucleotides		
For SMARTpool siRNA list please see Table S2	Dharmacon	N/A
For mouse primer sequences see Table S3	Sigma-Aldrich	N/A

(*Continued on next page*)

Continued

REAGENT or RESOURCE	SOURCE	IDENTIFIER
KASP Assay primer mix: TACTCTTATGAACCCGCGTACACGAC CCCGGGACCCCCGCTGGTGACCCA GCAGGACAGTCGCTTTCTCAGTG ATGCCGACATGG**[T/G]** GATGAGCTTTGCGAATAC AGGTGAGCGTCTTATGAAAT TCACCGCATATCATAATTG TTGTTAGGATGAATCAACA GATTGTTTTTGCTCCATT	Biosearch Technology (KASP by Design)	KBS-2100-100
bmp7b coding sequences	Zebrafish Information Network (ZFIN)	ZFIN-ID: ZDB-GENE-060929-328
bmp7a coding sequences	Zebrafish Information Network (ZFIN)	ZFIN-ID: ZDB-GENE-000208-25
Primer: *bmp7a* forward: 5′ TTGTGTACTCTTAT GAACCCGCGTA 3′	Eurofins Genomics	N/A
Primer: *bmp7a* reverse: 5′ GGAGCAAAAACAAT CTGTTGATTCA 3′	Eurofins Genomics	N/A
Tol2 transposase mRNA	Tol2 kit[86]	http://tol2kit.genetics.utah.edu/
Recombinant DNA		
pCS2P+ vector	Hammerschmidt lab	N/A
pENTR/D-TOPO	Thermo Fisher	K243520
pENTR-bmp7b	Stephan Heermann lab (this paper)	N/A
pDestTol2CG2	Tol2 kit[86]	http://tol2kit.genetics.utah.edu/
p5E-hsp70l	Tol2 kit[86]	http://tol2kit.genetics.utah.edu/
p3E-pA	Tol2 kit[86]	http://tol2kit.genetics.utah.edu/
Software and algorithms		
ImageJ	National Institutes of Health	https://imagej.net/
Image Lab 5.2.1	Bio-Rad Laboratories	https://www.bio-rad.com/it-it/product/image-lab-software

RESOURCE AVAILABILITY

Lead contact

Further information and requests for resources and reagents should be directed to and will be fulfilled by the lead contact, Gabriele D'Uva (gabrielematteo.duva2@unibo.it).

Materials availability

pENTR-*bmp7b* plasmid and *hsp70L*:bmp7b, *myl7*:eGFP^{af5Tg} transgenic zebrafish line are available at the laboratory where they were developed (Stephan Heermann lab, Institute of Anatomy and Cell Biology, Faculty of Medicine, University of Freiburg, Albertstrasse 17, 79104 Freiburg, Germany).

Data and code availability

- The raw data from all charts and western blot images have been deposited on Mendeley Data:https://doi.org/10.17632/8w43fgzdjx.1.
- This paper does not report original code.
- Any additional information required to reanalyze the data reported in this paper is available from the lead contact upon request.

EXPERIMENTAL MODEL AND STUDY PARTICIPANT DETAILS

Mice strains C57BL/6N and C57BL/6JRccHsd were maintained in ventilated cages under a 12:12 light:dark cycle at a controlled temperature, having *ad libitum* access to standard food and water. Sex-matched female and male C57BL/6N mice at postnatal day 1, 3, 7, 26 or 56 were used in this paper for *in vitro* studies, whereas female C57BL/6N mice at 2 months of age and C57BL/6JRccHsd at 3 months of age were used in this paper for *in vivo* studies. Experiments were approved by the Animal Care and Use

Committee of the University of Bologna (Italy), Cogentech Mouse Genetics Facility (IFOM, Milan, Italy) and Weizmann Institute of Science (Israel).

Female and male *hsp70L*:bmp7b, *myl7*:eGFP^{af5Tg} and *bmp7a*$^{ty68a/ty68a}$ (ZDB-ALT-980203-1308) zebrafish embryos or adults at 4–6 months of age were used in this paper. Experiments were approved by the state of Baden-Württemberg and animal care representatives of Ulm University. Fish were maintained in tanks under a 14:10 light/dark cycle at a controlled temperature.

METHOD DETAILS

Mouse cardiomyocyte isolation and culture

Primary neonatal cardiomyocytes were extracted from the hearts of 0-day-old or 1-day-old (P0-P1) mice. Neonatal cardiac cells were isolated by enzymatic digestion with pancreatin (Sigma) and collagenase (Roche), as previously described.[87] Primary juvenile cardiomyocytes were extracted from hearts of 7-day-old (P7) mice, which were anterogradely perfused with digestion enzymes (collagenase (Roche), trypsin (Sigma), and protease (Sigma)) as previously described.[88] Cells were then cultured in 0.1% gelatine-coated (Sigma) wells with DMEM/F12 (Aurogene) supplemented with 1% L-glutamine (Sigma), 1% sodium pyruvate (Life Technologies), 1% non-essential amino acids (Life Technologies), 1% penicillin and streptomycin (Euroclone), 5% horse serum (Invitrogen) and 10% FBS (Life Technologies) (hereafter referred to as 'complete-medium') at 37°C and 5% CO_2. The cells were allowed to adhere for 48 h in complete-medium (24 h for knockdown analysis). Subsequently, the medium was replaced with an FBS-deprived complete-medium containing selected growth factors (ImmunoTools) at the concentration of 10 ng/mL (or at the indicated concentrations in the figure legends), dosages in accordance with the usual range for *in vitro* experiments,[24,26,27,50,89,90] for about 48 h (for proliferation analyses) or 30, 60 and 120 min (for cell signaling analysis). For BrdU assays, BrdU (10 μM, B5002, Sigma) was introduced along with the treatments. For Western blot analysis, 24 h of starvation in the serum-deprived medium were performed before cell treatment.

Transient gene knockdown

To silence specific molecular targets, postnatal day 1 (P1) murine cardiomyocytes were isolated through enzymatic digestion and cultured in a complete medium, as described above. SMARTpool siRNAs (listed in Table S2), targeting *Bmpr1a* (L-040598-00-0005, Dharmacon), *Acvr1* (L-042047-00-0005, Dharmacon), *Acvr1b* (L-043507-00-0005, Dharmacon), *Acvrl1* (L-043004-00-0005, Dharmacon), *Bmpr2* (L-040599-00-0005, Dharmacon), *Acvr2a* (L-040676-00-0005, Dharmacon), *Smad1* (L-055762-00-0005, Dharmacon), *Smad5* (L-057015-01-0005, Dharmacon), *Smad9* (L-046344-01-0005, Dharmacon), and *Bmp7* (L-061990-01-0005, Dharmacon) were delivered to cardiomyocytes, 24 h post seeding, through Lipofectamine 3000 Transfection Reagent (L3000008, Thermofisher), following the manufacturer's protocol. Lipofectamine 3000 Reagent was used at the lowest recommended concentration. Gene knockdown was obtained following 48 h of transfection at 37°C and 5% CO_2. Subsequently, cells were lysed for RNA extraction, as described below, or the medium was replaced with an FBS-deprived complete-medium containing the selected growth factors (ImmunoTools) for 48 h (for proliferation assays).

Mouse cardiomyocyte and stromal cell separation

To separate cardiomyocytes and stromal cells in P1 and P7 hearts, we proceeded as follows. P1 hearts were subjected to enzymatic digestion, whereas P7 hearts were harvested and anterogradely perfused as described above. Cardiomyocytes were separated from stromal cells using the immunomagnetic cell sorting MACS Neonatal Isolation System (130-100-825, Miltenyi biotech), following the manufacturer's protocol. Enriched cardiomyocytes were then cultured in a complete medium. The validation of the enrichment procedure was previously demonstrated by the analysis of gene expression levels of markers specific for cardiomyocytes and stromal cells (fibroblasts and endothelial cells).[37] To assess changes in gene expression levels cardiomyocytes were centrifuged, and the total RNA was extracted from the pellet as described below.

Immunofluorescence on mouse cells and tissue sections

Cultured cells were fixed with 4% paraformaldehyde (PFA) solution (Sigma, diluted in PBS) for 20 min at 4°C or room temperature and then washed thrice in PBS. Heart sections (4 μm) underwent deparaffinization (by immersion in Toluene and rehydration by immersion in solutions with a decreasing concentration of Ethanol), and heat-induced antigen retrieval in EDTA buffer (Sigma) at pH 8.5 (for Ki67, phospho-SMAD1/5/9 and ERK2 immunostaining) or Sodium Citrate buffer (10mM Sodium Citrate, 0.05% Tween 20) at pH 6 (for Aurora B kinase and BrdU immunostaining), followed by gradual chilling. Then heart sections and cultured cells were processed in the following manner. Samples were permeabilized with 0.5% Triton X-100 (Sigma) in PBS for 5 min at room temperature and the non-specific binding of the antibodies was prevented by applying a blocking solution (PBS supplemented with 5% BSA (Sigma) or 5% goat serum (for Aurora B kinase immunostaining in heart sections) and 0.1% Triton X-100) for 1 h at room temperature. For the BrdU staining protocol on cultured cells, a DNA hydrolysis step between the permeabilization and the blocking step was performed by the addition of 2M HCL (Sigma) for 30 min at 37°C, followed by 3 washes in PBS. For the BrdU staining protocol on tissue section a DNA hydrolysis step directly after antigen retrieval was performed by the addition of 2M HCL (Sigma) in PBS for 30 min at 37°C, followed by a step of HCL neutralization with 0.1 M Borate Buffer pH 8.5 for 10 min at room temperature, 3 washes in PBS and incubation with blocking solution (PBS supplemented with 20% horse serum and 0.5% Triton X-100). Then samples were incubated

overnight at 4°C with primary antibodies diluted in PBS, supplemented with 3% BSA or 3% goat serum (for Aurora B kinase, phospho-SMAD1/5/9 and ERK2 analysis in heart sections) and 0.1% Triton X-100. For the BrdU staining protocol primary antibodies diluted in PBS, supplemented with 2% horse serum and 0.5% Triton X-100 were used. Anti-Troponin T (cTnT) (1:400, ab33589, Abcam) and anti-Troponin I (cTnI) (1:400, ab47003, Abcam) antibodies were used to identify cardiomyocytes. Anti-KI67 (1:50, ab16667, Abcam), anti-BrdU (1:40, G3G4, DSHB), and anti-Aurora B kinase (1:50, 611082, BD Transduction Laboratories) antibodies were used to analyze cell-cycle activity, DNA synthesis and cytokinesis, respectively. Anti-phospho SMAD 1/5/9 (1:500, 13820, Cell Signaling) and anti-ERK2 (1:50, sc-1647, Santa Cruz) were used to analyze BMP7 downstream signaling after myocardial infarction.

After primary antibody incubation, 3 washes in PBS were performed and the samples were incubated for 1 h at room temperature with fluorescent secondary antibodies, diluted (1:200) in PBS supplemented with 1% BSA, 1% goat serum (for Aurora B kinase, phospho-SMAD1/5/9 and ERK2 analysis in heart sections) or 1% horse serum (for BrdU analysis in heart sections) and 0.1% Triton X-100. For the BrdU staining protocol tissue sections were incubated for 90 min at room temperature with fluorescent secondary antibodies, diluted (1:200) in PBS supplemented with 2% horse serum. The following secondary antibodies were used: anti-mouse Alexa Fluor 488 (115-545-003, Jackson), anti-rabbit Alexa Fluor 488 (111-545-003, Jackson), anti-mouse Cy3 (115-165-003, Jackson), anti-rabbit 594 (AlexaFluor 111-585-003, Jackson), anti-rabbit Cy3 (111-165-003, Jackson). After 3 washes in PBS, DAPI (4′,6-diamidino-2-phenylindole dihydrochloride, Sigma), diluted at 1 μg/mL in PBS, was applied for 10 min at room temperature for nuclei visualization. 15 min of incubation were applied for the BrdU staining protocol on cultured cells. Samples were then washed 2 more times in PBS. Cells in the culture plates were imaged with the following widefield microscopies: Zeiss (Axio Observer A1), ArrayScan XTI (ThermoFisher), and Eclipse Ti2 (Nikon) at ×20 magnification. Slides were mounted with an antifade solution (Vectorlabs), covered with a coverslip, sealed with nail polish and imaged at an Olympus VS200 slide scanner at ×20 magnification. z stack images were acquired at Eclipse Ti2 (Nikon) with CrestOptics DeepSIM at ×60 magnification.

KI67, Aurora B kinase, BrdU, phospho-SMAD1/5/9 and ERK2 positive cardiomyocytes in tissue sections were counted manually within infarcted plus border zones or remote zones. For each heart an average value was calculated from the analysis of 1–3 sections per heart and then inserted in a boxplot. KI67 positive stromal cells in tissue sections were counted manually within infarcted plus border zones from 12 randomly selected circular areas; for each heart an average value was calculated from the analysis of 2–3 sections per heart and then inserted in a boxplot.

Protein extraction and western blotting

Western blotting was performed with the SDS–PAGE Electrophoresis System. Proteins were extracted from 400,000 to 500,000 cells with RIPA buffer with the addition of proteinase inhibitor (Sigma) and phosphatase inhibitors (Sigma). Then, 20–25 μg protein extracts were resolved by sodium dodecyl sulfate (SDS)-polyacrylamide gel electrophoresis and transferred to a nitrocellulose membrane (AmershamTM ProtranTM Premium 0.45 μm 300 mm × 4 m). The membrane was blocked for 1 h using TBS-T (0.1% Tween 20) supplemented by 5% BSA (Sigma), and incubated overnight at 4°C with the following primary antibodies: anti-SMAD1 (1:1000, 6944, Cell Signaling), anti-phospho SMAD1/5/9 (1:1000, 13820, Cell Signaling), anti-ERK2 (1:1000, sc-1647, Santa Cruz), anti-phospho-ERK (1:2500, M8159, Sigma), anti-AKT (1:1000, 9272, Cell Signaling), anti-phospho-AKT (1:1000, 9271, Cell Signaling), anti-GAPDH (1:1000, 2118, Cell Signaling) and anti-α-tubulin (1:4000, T5168, Sigma). For protein detection, the membrane was incubated with anti-rabbit or anti-mouse horseradish peroxidase-labelled secondary antibody (Dako EnVision+ System- HRP Labeled Polymer) followed by a chemiluminescent reaction (Clarity Western ECL Substrate, Bio-Rad). Signals and images were acquired by ChemiDoc XRS 2015 (Bio-Rad Laboratories), and densitometric analysis were performed using Image Lab software (version 5.2.1; Bio-Rad Laboratories).

Transcriptional analysis

Total RNA extraction was performed with the NucleoSpin RNA II kit (Macherey Nagel) according to the manufacturer's protocol. RNA quantification and quality check were performed using a Nanodrop spectrophotometer (N1000, Thermo). RNA was reverse transcribed to double-stranded cDNA using SuperScript VILO cDNA Synthesis Kit (Invitrogen) according to the manufacturer's protocol. Real-Time (rt)-PCR was performed using Fast SYBR Green PCR Master Mix (Applied Biosystems) on a QuantStudio 6 Flex instrument (Applied Biosystems) and a QuantStudio 5 Flex instrument (Applied Biosystems). Oligonucleotide sequences of genes analyzed in this study namely *Bmp7*, *Bmpr1a*, *Bmpr2*, *Acvr2a* and *Acvr1*, are listed in Table S3. Relative quantification was performed using the Hprt1 gene as a loading control. DDCT was calculated and data of each gene were analyzed using a 2^{-DDCT} method and reported as mean fold change.

Time-lapse imaging

Following cell isolation, postnatal day 1 (P1) cardiomyocytes were seeded at 35,000 cells per well in a 96-well plate and left to adhere for 48 h. Then, the complete medium was replaced with serum-free medium supplemented with 10 nM TMRE (tetramethylrhodamine ethyl ester, Sigma), a fluorescent mitochondrial dye used to label cardiomyocytes.[54] After 20 min of incubation at 37°C, the medium containing TMRE was removed, and cardiomyocytes were treated with and without BMP7 (ImmunoTools) at 10 ng/mL in FBS-deprived complete medium. Live cell imaging was performed using a widefield fluorescent microscope (Nikon Eclipse TI2). Time-lapse imaging was carried out for 16 h and images were acquired at ×40 magnification every 15 min.

Myocardial infarction in the mouse model

Myocardial infarction in the adult stage was induced by ligation of the left anterior descending coronary artery as previously described.[24] Female 3-months old C57BL/6JRccHsd mice were sedated with isoflurane (Abbott Laboratories) and artificially ventilated following tracheal intubation. Lateral thoracotomy at the fourth intercostal space was performed by blunt dissection of the intercostal muscles following skin incision. After the ligation of the left anterior descending coronary artery, thoracic wall incisions were sutured with 6.0 non-absorbable silk sutures, and the skin wound was closed using glue. Mice were then warmed for several minutes until recovery.

In vivo drug delivery in the mouse model

For myocardial infarction models, two days after damage, Recombinant Human BMP7 (Peprotech) was delivered on a daily basis with a dose of 100 μg/kg/day dissolved in water for 12 days, through IV (intravenous) injection every 3 days and IP (intraperitoneal) injection for the rest of the time up to 14 days after myocardial infarction. The administration method and the selected dose of the growth factor are similar to previous reports.[23] Infarcted control mice were subjected to daily injections of water for 12 days. At the end of the treatment, mice were sacrificed, and hearts were collected for analysis of cardiac cell proliferation (KI67, Aurora B kinase and BrdU staining) or BMP7 downstream pathways (phospho-SMAD1/5/9, ERK2 and AKT staining). For the BrdU staining protocol 50 mg kg^{-1} BrdU were injected at day 3, 5 and 7 post-myocardial infarction. For uninjured mouse models, Recombinant Human BMP7 (Peprotech) was delivered daily with a dose of 100 μg/kg/day dissolved in water for 12 days, through IV (intravenous) injection every 3 days and IP (intraperitoneal) injection for the rest of the time. Control mice were subjected to daily water injection. At the end of the treatment, mice were sacrificed, and hearts were collected for analysis of cardiac cell cycle activity (KI67 staining).

Rescue of zebrafish *bmp7a* (snailhouse) mutants

We previously reported that *bmp7* expression is induced after ventricular cryoinjury of adult zebrafish hearts.[57] Please note that the transcript termed "*bmp7*" in our previous publication[57] has in the meantime been re-named *bmp7a* by the zebrafish nomenclature committee. We used the following previously identified *bmp7a* loss-of-function allele in the present study: snh (snailhouse)^{ty68a}.[58]

To test the efficacy of zebrafish *bmp7a* and *bmp7b* to rescue the early developmental defects of *bmp7a* homozygous mutants, the *bmp7a* and *bmp7b* coding sequences (ZDB-GENE-000208-25 and ZDB-GENE-060929-328 respectively) were cloned into the pCS2P+ vector. Capped sense RNA was synthesized from linearized plasmids using mMessage mMachine kit (Invitrogen) and RNA was purified using RNeasy Mini kit (Qiagen). 300 pg of *bmp7a* or *bmp7b* mRNA was injected into embryos derived from incrosses of *bmp7a*^{ty68a} heterozygous carriers at the 1 cell stage. Injected embryos were allowed to grow until 3 dpf (days post fertilization), at which stage all non-rescued homozygous mutant embryos would have died. Genomic DNA was isolated from single embryos using NaOH, diluted 1:6 in nuclease free H_2O and 5 μL were used for Kompetitive allele specific PCR (KASP) genotyping (LGC Biosearch Technology). Cycling program for KASP PCR included a hot-start activation at 94°C for 15 min, 10 cycles at 94°C for 20 s and at 61°C for 60 s, 26 cycles at 94°C for 20 s and at 55°C for 60 s, followed by 3 cycles at 94°C for 20 s and at 57°C for 60 s. The 2X KASP Master mix and KASP Assay primer mix were designed and provided by LGC Biosearch Technology (KASP by Design) using TACTCTTATGAACCCGCGTACACGACCCCGGGACCCCCGCTGGTGACCCAGCAGGACAGTCGCTTTCTCAGTGATGCCGACATG G**[T/G]**GATGAGCTTTGCGAATACAGGTGAGCGTCTTATGAAATTCACCGCATATCATAATTGTTGTTAGGATGAATCAACAGATTGT TTTTGCTCCATT for each allele in which the FAM fluorophore (T) corresponds to the wild type allele and the HEX fluorophore (G) corresponds to the mutated one. The rescue efficiency was calculated by dividing the % mutant genotype by the % expected mutant genotype after complete rescue.

To generate *bmp7a* homozygous mutants for adult experiments, embryos derived from incrosses of snh^{ty68a} heterozygous carriers were injected with 300 pg of *bmp7a* mRNA, raised to adulthood and homozygous fish were identified by sequencing. To this end, a fragment of the *bmp7a* locus was amplified by PCR using the primers 5′ TTGTGTACTCTTATGAACCCGCGTA 3' (sense) and 5′ GGAGCAAAAACAATCTGTTGATTCA 3' (antisense) and PCR products were sequenced using the sense primer. The ty68a allele contains a single T-to-G point mutation: the wild-type sequence is GTG (coding for Valine), the mutant sequence is GGG (coding for Glycine). Adult tanks contained on average 12% homozygous mutant fish; thus we were able to rescue about half of the expected homozygous mutant embryos (25% of the total).

Phenotypic comparison between *bmp7a* and *bmp7b* overexpression models

To compare the biological activity of zebrafish *bmp7a* and *bmp7b* when overexpressed, 300 pg of *bmp7a* or *bmp7b* mRNA was injected into zebrafish embryos derived from wild-type outcrosses at the 1 cell stage. Phenotype analysis was performed at 24 hpf (hours post fertilisation) and classified into the V1-V4 ventralisation classes scheme according to previously published data.[91]

Generation of *hsp70L*:bmp7b, *myl7*:eGFP^{af5Tg} transgenic zebrafish line

The following transgenic line for heat-shock-inducible overexpression of zebrafish *bmp7* and concomitant labeling of cardiomyocytes by eGFP was created for this publication: *hsp70L*:bmp7b, *myl7*:eGFP^{af5Tg}. To this end the coding sequence of *bmp7b* (ZFIN-ID: ZDB-GENE-060929-328) was amplified from cDNA and cloned into pENTR/D-TOPO (Thermo Fisher). The transgenesis construct was generated by Multiway Gateway (Thermo Fisher) cloning using pENTR-bmp7b, as well as p5E-hsp70l, p3E-pA, and pDestTol2CG2 from the Tol2 kit.[86] AB wild type embryos were injected with *hsp70L*:bmp7b, *myl7*:eGFP plasmid and Tol2

transposase mRNA, screened for *myl7*:GFP expression, and raised to adulthood. Mosaic F0 adults were crossed with AB wild type fish to obtain heterozygous Tg(*hsp70L*:bmp7b, *myl7*:GFP) zebrafish.

Zebrafish heart cryoinjuries, EdU injection and heat-shocks

Cryoinjuries were performed as previously described on zebrafish of 4–6 months of age,[57] except that a liquid nitrogen-cooled copper filament of 0.3-mm diameter was used instead of dry ice. In experiments involving *bmp7a* loss-of-function, fish were injected intraperitoneally with 10 μL of 10 mM 5-ethynyl-2-deoxyuridine (EdU) in PBS once daily for 3 days, starting 4 days after cryoinjury, and cycling of cardiomyocytes (detected by anti-MHC immunofluorescence) was evaluated at 7 days post injury. For heat-shock-inducible overexpression of *bmp7b*, *hsp70L*:bmp7b, *myl7*:eGFP^{af5Tg} transgenic fish were heat-shocked once daily for 6 days, starting at 1 day post cryoinjury (dpi), or for 7 days in uninjured models, and analyzed 5 h after the end of the last heat shock at 7 dpi. To apply heat-shocks, water containing fish was heated to 37°C for 1 h, after which the water temperature was reduced back to 27°C within 15 min. Wild-type negative control fish were heat-shocked as well.

Immunofluorescence on zebrafish tissue sections

Zebrafish hearts were fixed in 4% paraformaldehyde (PFA) (in phosphate buffer with 4% sucrose) at room temperature for 1 h, washed three times for 10 min in 4% sucrose/phosphate buffer and equilibrated in 30% sucrose/phosphate buffer overnight at 4°C. Hearts were embedded and cryosectioned into 10-μm sections. Sections were equally distributed onto six serial slides so that each slide contained sections representing all areas of the ventricle. Immunostainings were performed as previously described.[92] The following primary antibodies were used: anti-PCNA (1:1000, M0879, RRID:AB_2160651, Dako), anti-MF20 (which detects sarcomeric Myosin heavy chain – MHC; 1:50, MF20, RRID:AB_2147781, Developmental Studies Hybridoma Bank), anti-Myl7 (1:300, GTX128346, RRID:AB_2885759, Genetex), anti-phospho Smad1/5/9 (1:500, 13820 D5B10, Cell Signaling). Secondary antibodies conjugated to Alexa 488, 555 or 633 (Invitrogen) were used at a dilution of 1:1000. Nuclei were shown by DAPI (40,60-diamidino-2-phenylindole) staining.

For EdU detection, cryosections were prepared the same way as for immunofluorescence staining. Slides were washed twice in 3% BSA/PBS for 5 min, once in 0.5% Triton X-100/PBS for 20 min, and twice in 3% BSA/PBS for 3 min each. Slides were incubated in the dark with the reaction cocktail (EdU-Imaging kit, baseclick GmbH) as per manufacturer's protocol for 30 min. Slides were washed for 3 min in 3% BSA/PBS and subjected to the immunofluorescence protocol to detect MHC (MF20) as described above.

All images of immunofluorescence staining are single optical planes acquired using 20× magnification with a Zeiss AxioObserver 7 equipped with an Apotome or with Leica Sp5 or Sp8 confocal microscopes. Quantifications of the fraction of EdU or PCNA positive cardiomyocytes were performed on 2 to 3 sections with the biggest wounds per heart and in cardiomyocytes located within 150 μm from the wound border. EdU+ or PCNA+ cardiomyocytes were counted manually within this border zone area. The number of cardiomyocytes in the wound border zone was estimated by multiplying the wound border area size (measured using ImageJ) with the average density of cardiomyocytes in three separate regions of interest (size: 100 μm^2) within the border zone area, which was determined by counting cardiomyocyte nuclei within the regions of interest. For each heart the average value was calculated from the analysis of 2–3 sections per heart.

QUANTIFICATION AND STATISTICAL ANALYSIS

Whenever normality could be assumed, the two-sided Student's t-test or analysis of variance (ANOVA) followed by Sidak's, Tukey's and Dunnet's test were used to compare group means, as specified in the figure legends. p value < 0.05 was considered to represent a statistically significant difference. In all panels, numerical data are expressed as mean + standard error of the mean (s.e.m.). For phenotypic analysis of zebrafish embryos, Chi-squared test has been used. Statistical analyses were performed using GraphPad Prism software. Every dot represents a different biological replicate, as indicated in the figure legends, together with the number of cardiac cells analyzed.